1 **TITLE**

2 Precise Therapeutic Targeting of Distinct *NRXN1*$^{+/-}$ Mutations

3 **AUTHORS**

4 Michael B. Fernando[1,2,4,5], Yu Fan[3]*, Yanchun Zhang[3]*, Sarah Kammourh[3], Aleta N. Murphy[1,2,4],
5 Sadaf Ghorbani[5,6], Ryan Onatzevitch[2], Adriana Pero[3], Christopher Padilla[3], Lei Cao[3], Sarah
6 Williams[1-4], Gang Fang[3#], Paul A. Slesinger[2#] & Kristen J. Brennand[2-5#]

7 **AFFILIATIONS**

8 [1] Graduate School of Biomedical Science, Icahn School of Medicine at Mount Sinai, New York,
9 NY 10029

10 [2] Nash Family Department of Neuroscience, Icahn School of Medicine at Mount Sinai, New York,
11 NY 10029

12 [3]Department of Genetics and Genomics, Icahn School of Medicine at Mount Sinai, New York, NY
13 10029

14 [4]Friedman Brain Institute, Black Family Stem Cell Institute, Pamela Sklar Division of Psychiatric
15 Genomics, Icahn School of Medicine at Mount Sinai, New York, NY 10029

16 [5] Department of Psychiatry, Yale School of Medicine, New Haven, CT, 06520

17 [6]Haukeland University Hospital, Bergen, Norway

18 *These authors contributed equally

19 [#]Correspondence: kristen.brennand@yale.edu, paul.slesinger@mssm.edu and
20 gang.fang@mssm.edu

21 **KEYWORDS**

22 Human induced pluripotent stem cells; *NRXN1*; alternative splicing; glutamatergic neurons;
23 GABAergic neurons; genomics; neuropsychiatric disorder; disease modeling; precision medicine

ABSTRACT

As genetic studies continue to identify risk loci that are significantly associated with risk for neuropsychiatric disease, a critical unanswered question is the extent to which diverse mutations --sometimes impacting the same gene-- will require common or individually tailored therapeutic strategies. Here we consider this in the context of rare, heterozygous, and non-recurrent copy number variants (2p16.3) linked to a variety of neuropsychiatric disorders that impact *NRXN1*, a pre-synaptic cell adhesion protein that serves as a critical synaptic organizer in the brain. Complex patterns of *NRXN1* alternative splicing are fundamental to establishing diverse neurocircuitry, vary between the cell types of the brain, and are differentially impacted by unique patient-specific (non-recurrent) deletions. Progress towards precision medicine may require restoring each person's *NRXN1* isoform repertoires in a cell-type-specific manner**.** Towards this, here we contrast the cell-type-specific impact of unique patient-specific mutations in *NRXN1* using human induced pluripotent stem cells. Perturbations in *NRXN1* splicing causally lead to divergent cell-type-specific synaptic outcomes: whereas *NRXN1*$^{+/-}$ deletions result in a decrease in synaptic activity throughout glutamatergic neuron maturation, there is an unexpected increase in synaptic activity in immature GABAergic neurons. Both glutamatergic and GABAergic synaptic deficits reflect independent loss-of-function (LOF) and gain-of-function (GOF) splicing defects. Towards clinical relevance, we show that treatment with β-estradiol increases *NRXN1* expression in glutamatergic neurons, while antisense oligonucleotides knockdown mutant isoform expression across both glutamatergic and GABAergic neurons. Direct or indirect manipulation of *NRXN1* splicing isoforms provides a promising therapeutic strategy for treating humans with 2p16.3 deletions.

MAIN

Neurexins are pre-synaptic cell adhesion proteins that act as a synaptic organizer (*1*). There are three neurexin genes (*NRXN1*, *NRXN2*, and *NRXN3*) in mammals and each is highly alternatively spliced to produce hundreds of isoforms, primarily categorized into long alpha and shorter beta isoforms (*2*). The complex alternative splicing of neurexins allows for widespread expansion of protein-protein interaction capabilities (*3*), providing the basis for neurexins to interact with diverse post-synaptic ligands to establish and maintain neurotransmission. *NRXN1*α splice variants are specific to brain regions (*4*) and between cell types (*5*), but the cell-type-specific functional impact of individual isoforms remains unclear. Although rare in the population, large copy number variations (deletions or duplications) at the *NRXN1* locus 2p16.3, particularly those deleting exonic regions are highly penetrant, pleiotropic, and are strongly associated with several

56 neuropsychiatric diseases, including schizophrenia (odds ratio 14.4(ref. *6*)), autism spectrum
57 disorder (odds ratio 14.9 (ref. *7*)), epilepsy (odds ratio 9.91 (ref. *8*)), intellectual disability (odds
58 ratio 7.47 (ref. *9*)) and Tourette's syndrome (odds ratio 20.3 (ref. *10*)). These exonic deletions in
59 *NRXN1* are non-recurrent (that is, they vary in size and location), making it difficult to determine
60 the molecular mechanisms underlying their diverse clinical symptoms (e.g., diagnosis, severity,
61 prognosis, and age-of-onset). In rodent studies, gene knock outs (KO) of each *NRXN(1-3)* is
62 sufficient to produce an array of excitatory and inhibitory synaptic phenotypes (*1*). However,
63 heterozygous KO produce modest behavioral and physiological changes *in-vivo (11)*. By
64 contrast, however, *in-vitro* studies of engineered heterozygous $NRXN1^{+/-}$ human neurons reveal
65 robust changes in excitatory neurotransmission that are not observed in matched $NRXN1^{+/-}$
66 mouse neurons (*12, 13*). While these studies do not evaluate how $NRXN1^{+/-}$ impacts the complex
67 alternative splicing of the gene or the non-recurrent nature of the deletions, they collectively
68 suggest that neurexins possess unique human neurobiology, and therefore, the impact of the
69 distinct patient-specific $NRXN1^{+/-}$ must be specifically evaluated in human models.

70 Human induced pluripotent stem cell (hiPSC)-derived neurons provide an ideal platform to study
71 *NRXN1α* alternative splicing. Previously we established that hiPSC-derived forebrain cultures,
72 comprised of a mixture of glutamatergic and GABAergic neurons with residual astroglia,
73 recapitulate the diversity of *NRXN1α* alternative splicing observed in the human brain, cataloguing
74 123 high-confidence *NRXN1α* isoforms (*14*). Furthermore, using patient-derived $NRXN1^{+/-}$
75 hiPSCs with unique 5' or 3' deletions in the gene, we uncovered wide-scale reduction in wildtype
76 *NRXN1α* isoform levels and, robust expression of dozens of novel isoforms from the 3' mutant
77 allele (*14*). Overexpression of individual wildtype isoforms ameliorated reduced neuronal activity
78 in patient-derived $NRXN1^{+/-}$ hiPSC-neurons in a genotype-dependent manner, whereas mutant
79 isoform expression decreased neuronal activity levels in control hiPSC-neurons (*14*). We
80 therefore hypothesized that 5' deletions of the promoter region represent classical loss-of-function
81 (LOF), while robust expression of 3' specific novel mutant isoforms can confer a gain-of-function
82 (GOF) effect that cannot be rescued by overexpression of wildtype isoforms. Although *NRXN1*
83 splicing varies between the cell types of the brain, the impact of non-recurrent $NRXN1^{+/-}$ deletions
84 on cell-type-specific splicing patterns and synaptic function remains untested.

85 Given the multifaceted role of *NRXN1* in excitatory and inhibitory synapses, the lack of
86 mechanistic understanding of how aberrant splicing impacts neuronal physiology in a cell-type
87 *and* genotype-dependent manner presents a significant challenge for therapeutic targeting. To
88 discover the disease mechanisms that underpin $NRXN1^{+/-}$ deletions, we leverage advanced 2D

89 lineage conversion, and 3D organoid models to simultaneously compare excitatory and inhibitory
90 neurons across 5' LOF and 3' GOF deletions. We identified points of phenotypic divergence
91 across glutamatergic and GABAergic neurons, which were independently validated in isogenic
92 experiments to establish causal relationships between aberrant splicing and synaptic dysfunction.
93 Finally, we inform and test the design of novel therapeutic agents for *NRXN1*$^{+/-}$ deletions on
94 LOF/GOF stratified patient mechanisms.

95

96 **RESULTS**

97 **Shared aberrant splicing in patient-specific glutamatergic and GABAergic neurons.**

98 To examine the impact of *NRXN1*$^{+/-}$ deletions in two different neuronal cell types, we used lineage
99 conversion of patient hiPSCs for generating either excitatory glutamatergic neurons or inhibitory
100 GABAergic neurons. Transient overexpression of *NGN2* in hiPSCs produces iGLUT neurons that
101 are >95% pure glutamatergic neurons, robustly express glutamatergic genes, release glutamate,
102 and produce spontaneous synaptic activity by day 21 in vitro (*15-18*). On the other hand, transient
103 overexpression of *ASCL1* and *DLX2* yields iGABA neurons that are >80% positive for expressing
104 GABA and GAD1/2 by day 35 in vitro, and possess mature physiologic properties of inhibitory
105 neurons by day 42 (*16, 19*). We combined these highly efficient iGLUT and iGABA induction
106 protocols with hiPSCs from patients with rare heterozygous intragenic deletions in *NRXN1* (*14*).
107 Two cases containing the same ~136-kb deletion in the 3'-region of *NRXN1* (3' del) and two cases
108 with ~115-kb deletions in the 5'-region of *NRXN1* (5'-Del). For controls, we used four passage-
109 matched and sex-balanced subjects (**Fig. 1a,b**). Immunostaining confirmed expression of
110 neurotransmitter transporters, vGLUT1 and vGAT for iGLUT and iGABA neurons, respectively
111 (**Fig. 1c,h**). RNA-sequencing (RNAseq) further validated iGLUT (DIV21) and iGABA (DIV35)
112 neuronal induction in all donors (**Fig. 1d,i**).

113 We first compared the transcriptomics of *NRXN1*$^{+/-}$ deletions with controls for both iGLUT and
114 iGABA neurons. RNAseq analyses revealed overlap of the top differentially expressed genes
115 (DEGs) across cell types/genotypes (e.g., *FAM66D, TTC34, GALNT9*), whereas the majority of
116 case/control DEGs were genotype-specific (**Fig. 1e,j**). Gene-ontology analyses revealed a robust
117 enrichment of developmental and synaptic terms for the 5'-Del iGLUT condition over all other
118 conditions. Using publicly curated gene lists (*20, 21*), risk enrichments for schizophrenia, bipolar
119 disorder, and autism spectrum disorder were most enriched in iGLUT neurons from 5'-Del cases

120 and iGABA neurons from 3'-Del cases (**Fig. 1f,k and Extended Data Fig. 2**). Baseline
121 transcriptional comparisons therefore suggested the potential of strong phenotypes for 5'-Del
122 iGLUT neurons. Despite cell-type-specific *NRXN1* isoform profiles reported in healthy brains (*5*)
123 and neurons (*14*), aberrant *NRXN1* alpha/beta exon usages were shared between *NRXN1*$^{+/-}$
124 iGLUT and iGABA neurons (**Fig. 1g,l**), whereby alpha exon usage decreased for 5'-Del and
125 increased for 3'-Del in both types of neurons. These observations with specific iGLUT and iGABA
126 neurons parallel those from our previous study using hiPSC-derived forebrain neurons, which was
127 a mixture of glutamatergic and GABAergic neurons with astroglia (*14*).

128 **Patient-specific alterations in spontaneous neural activity occur without changes in**
129 **passive and excitable membrane properties.**

130 To evaluate the functional consequence of *NRXN1*$^{+/-}$ deletions on neuronal activity, we conducted
131 a population-level analysis of spontaneous neuronal activity using a multi-electrode array (MEA)
132 with 5'-Del, 3'-Del or control neurons co-cultured with primary mouse glial cells for six weeks to
133 promote maturation. Interestingly, spontaneous network activity (weighted mean firing rate,
134 wMFR) in *NRXN1*$^{+/-}$ iGLUT neurons was reduced by over 40% in two independent time points, at
135 weeks post induction (WPI) 4 and 6 (**Fig. 2a-c,** 5'-Del p=0.0011; 3'-Del, p<0.0001, 1-way ANOVA,
136 Dunnet's test). We next examined the passive membrane properties using whole-cell patch-clamp
137 electrophysiology. The cell capacitance, membrane resistance and resting membrane potentials
138 did not significantly differ between 5'- and 3'-Del cases and control iGLUT neurons (**Fig. 2d**). To
139 examine the intrinsic excitability, we compared the input-output curve for induced firing and found
140 no statistical difference in the maximal number of evoked action potentials (**Fig. 2e,** 2-way
141 ANOVA, Dunnett's test). Furthermore, the voltage-dependent sodium and potassium current
142 densities were similar between 5'-Del, 3'-Del and control iGLUT neurons (**Extended Data Fig**.
143 **3a**). Taken together, these results suggest that changes in passive or intrinsic excitability
144 membrane properties cannot explain the reduced firing observed on MEAs for 5'-Del and 3'-Del
145 in iGLUT neurons.

146 In parallel, we generated iGABA neurons with the same 5'-Del, 3'-Del, and control hiPSCs, as
147 above. We observed that immature *NRXN1*$^{+/-}$ iGABA neurons exhibited a robust ~2-fold increase
148 in population-wide wMFR activity (WPI2-3) from both 5'-Del and 3'-Del cases (5'-Del p=0.0381;
149 3'-Del, p=0.0047, 1-way ANOVA, Dunnet's test) (**Fig. 2f,g**). Though unexpected for GABA
150 neurons, the finding is consistent with activation of ionotropic GABA receptors leading to
151 depolarization due to little KCC2 expression and reduction of internal chloride levels (*22*). Indeed,

152 immature iGABA neurons expressed higher (10-fold increase compared to WPI2 neurons) levels
153 of *SLC12A5* (the gene encoding *KCC2*) (**Extended Data Fig. 4a** $p<0.0001$, 2-way ANOVA,
154 Dunnet's test). Furthermore, this transient hyperexcitability was pharmacologically inhibited by
155 10μM gabazine, a selective $GABA_A$ antagonist (**Extended Data Fig. 4b,c**). In mature iGABA
156 neurons (>5 weeks), post-*KCC2* switch, the average wMFR decreased in 5'-Del and 3'-Del
157 neurons (5'-Del p=0.0809; 1-way ANOVA, Dunnet's test) (**Fig. 2h**). Like iGLUT neurons, the
158 passive and intrinsic excitability membrane properties of iGABA neurons were not different
159 between *NRXN1*$^{+/-}$ 5'-Del or 3'-Del and controls (**Fig. 2i-j**, **Extended Data Fig. 3b**).

160 Overall, these data suggest that patient-specific changes in spontaneous neural activity are not
161 driven by differences in passive and excitable membrane properties in iGLUT or iGABA neurons
162 from *NRXN1*$^{+/-}$ 5'-Del and 3'-Del patients. Furthermore, these deletions did not appear to alter
163 maturation of iGLUT or iGABA neurons, as evidenced by similar induced firing rates and resting
164 membrane potentials.

165 ***NRXN1*$^{+/-}$ 5' and 3' deletions result in divergent synaptic transmission deficits.**

166 To further dissect the factors mediating phenotypes in altered spontaneous firing, we next
167 investigated the efficacy of synaptic transmission in iGLUT and iGABA neurons. Voltage-clamp
168 recordings of spontaneous excitatory post-synaptic currents (sEPSCs, no TTX) in iGLUT neurons
169 revealed decreased frequency of events for both for 5'-Del and 3'-Del cases (**Fig. 3a**). The
170 cumulative probabilities of inter-event-intervals (IEI) for both 3'-Del (P= 1.27E-11, Levene's test)
171 and 5'-Del iGLUTs (5'-del P= 2.44E-5) (**Fig. 3a,b**) was significantly increased, compared to
172 controls. The sEPSC amplitude increased for 5'-Del neurons (**Fig. 3a,c**). Miniature excitatory
173 post-synaptic currents (mEPSCs, +TTX) showed similar trends in IEI but no changes in amplitude
174 sizes across genotypes (IEI 5'-del P =0.0411, 1-way ANOVA, Dunnett's test) (**Extended Data**
175 **Fig. 5a,b**). These reductions in synaptic transmission are consistent with the transcriptomic
176 signatures; pre-synaptic (SynGO) genes showed a larger change (than post-synaptic) in synaptic
177 gene expression signatures (5'-del Pre-SynGO, Log_2FC = 0.1252; 3'-del Pre-SynGO, Log_2FC= -
178 0.0156) (**Fig. 3d,e**). We further probed transcriptional signatures of known *NRXN1* trans-synaptic
179 interaction partners that mediate synapse formation, function, plasticity and are frequently linked
180 with neuropsychiatric disease (*23*), and found they were represented in DEGs, including *CBLN2*,
181 *LRRTM4* and *NXPH1*, suggesting these synaptic effects are largely driven by change in *NRXN1*
182 expression (**Fig. 3f**).

183 By contrast, synaptic transmission in iGABA neurons appeared to be enhanced. The frequency
184 of spontaneous inhibitory post-synaptic currents (sIPSCs) increased, marked by a significant
185 decrease in IEI in 3'-Del iGABA neurons (3'-del P= 0.050E-5 by Levene's test) (**Fig. 3g-i)**. There
186 was no change in sIPSC amplitude (**Fig. 3i**). Miniature inhibitory post-synaptic currents (mIPSCs)
187 recorded in the presence of TTX and CNQX (AMPA/Kinate receptor antagonist) revealed similar
188 trends in IEI, with no change in mIPSC amplitudes (**Extended Data Fig. 5c-d**). Similarly, SynGO
189 analysis revealed concordant changes in synaptic transmission and transcriptomic signatures at
190 3'-del Pre-SynGO (Log_2FC = 0.0324), and represented of DEGs among *NRXN1* trans-synaptic
191 interaction partners *CBLN2*, *NLGN1*, *NXPH1, CASK,* and *LRRTM2-4* (**Fig. 3j-l)**.

192 Overall, patient-specific alterations in spontaneous neural activity were driven by synaptic deficits,
193 with the cell type-specific impact of aberrant *NRXN1* splicing resulting in divergent
194 neurotransmission phenotypes. Furthermore, non-recurrent LOF and GOF presented unequal
195 effect sizes between cell-types, with 5'-Del neurons being most impacted by excitatory
196 transmission, but 3'-Del neurons being affected by both excitatory and inhibitory transmission.
197 Given that deletions affected iGLUT and iGABA neurons in opposing directions, these findings
198 may implicate *NRXN1* as a key mediator of excitatory/inhibitory balance, a prevalent theme
199 among neuropsychiatric disorders (*24*).

200 **Region-specific organoids resolve non-autonomous defects of neurogenesis and**
201 **neuronal development.**

202 To explore the impact of aberrant *NRXN1* splicing on neural patterning (*25*) within a self-
203 organized microenvironment, we applied dorsal forebrain patterning to yield 5'-Del, 3'-Del and
204 control human cortical organoids (hCOs) that resemble the pallium, or applied ventral forebrain
205 patterning to generate human subpallial organoids (hSOs) that resemble the subpallium (**Fig.**
206 **4a,h**) (*26, 27*). Organoid sizes varied at early time points, but maintained consistency across
207 genotypes by 4 months (**Extended Data Fig. 6a,b,g,h**). RT-qPCR validated dorsal and ventral
208 patterning, and further confirmed robust expression of mutant isoforms exclusively from the 3'-
209 Del patients, with no expression from 5'-Del and control organoids (**Extended Data Fig. 6c-e, i-**
210 **k**). To unbiasedly characterize transcriptomics of cortical and subpallial organoids, we performed
211 single cell RNA-seq (n = 47,460 cells from hCOs, n= 35,563 cells from hSOs using 10x genomics)
212 at 6 months, a timepoint with well characterized neural activity (*26, 28*). We identified subclusters
213 of cell-types within hCOs and hSOs (**Fig.4b,i**), and confirmed consistent distributions of cell
214 clusters across genotypes (**Fig. 4c,j**). Strong expression of *NRXN1* and *FOXG1* confirmed

215 forebrain identity (and excluded one of six cell lines), while *EMX1* expression confirmed
216 dorsalization of remaining hCOs. Likewise, *DLX2* expression confirmed ventralization of hSOs,
217 with an enrichment of GABAergic-fated neurons (**Fig. 4d,k**).

218 A recent study demonstrated that KO of *NRXN1* increased replication of NPCs in human cells
219 and in the *xenopus* telencephalon (*29*). To test if *NRXN1*$^{+/-}$ deletions could impact neurogenesis,
220 we quantified neural rosette proliferation detected with immunofluorescence by calculating the
221 ratio of *KI67* protein to *SOX2* protein expression, as markers of proliferative cells and multipotent
222 neural stem cells. In the hCO subtype (DIV55-62), 3'-Del patient rosettes exhibited increased
223 KI67:SOX2 compared to control (P= 0.0063, by 1-Way ANOVA) (**Fig. 4e-f**), while in the hSO
224 subtype, 5'- and 3'-Del rosettes had reduced *KI67:SOX2* ratios (5'-del P= 0.0004; 3'-del P=
225 0.0004, by 1-Way ANOVA) (**Fig. 4l-m**). These results may explain the variation in NPC:neuron
226 proportions across genotypes (**Fig. c,j**). Differentially expressed gene sets identified cell-type-
227 specific effects in hCO-glutamatergic, hSO-GABAergic, and astroglia clusters, with robust
228 enrichment of GO terms related to RNA splicing (from upregulated genes), and
229 neurodevelopment and synaptic function (from downregulated genes) (**Fig. 4g,n**). Much of the
230 enriched GO terms overlapped among hCO-glutamatergic and hSO-GABAergic neurons, and
231 unexpectedly certain GO terms also reached significance in hCO-astroglia, but not hSO-astroglia
232 clusters (**Extended Data Fig. 7**). Overall, these data suggest that patterns of divergent cell-type
233 specific effects, particularly at the level of neural precursor states, persisted in our 3D models of
234 forebrain development, resulting in significant changes to glutamatergic and GABAergic neurons.

235 **Isogenic validation of divergent synaptic deficits, and therapeutic targeting of stratified**
236 **patients.**

237 To further support our findings of opposing, cell-type-specific changes in glutamatergic and
238 GABAergic synaptic transmission, with unequal effect size between non-recurrent *NRXN1*
239 deletions, we utilized a more direct approach using isogenic lines to causally link aberrant splicing
240 to synaptic dysfunction and develop candidate therapies (**Fig. 5a,h**). First, we utilized short hairpin
241 RNAs (shRNAs) to knockdown wildtype or mutant splice isoforms to mimic LOF or rescue GOF
242 phenotypes, respectively. Targeted knockdown of constitutively expressed exon 9 (expressed in
243 all alpha isoforms but not beta isoforms) achieved mRNA knockdown of ~55% in iGLUT neurons,
244 and ~75% in iGABA neurons across two or more isogenic pairs (compared to a non-targeting
245 control shRNA) (**Extended Data Fig. 8**). In iGLUT neurons, we observed decreased synaptic
246 transmission (i.e., increased sEPSC IEI, P= 2.2E-16 by Levene's Test) (**Fig. 5b,c**), whereas in

247 iGABA neurons we observed increased synaptic transmission (decreased IEI, P = 2.2E-16 by
248 Levene's Test and P= 0.0250 by 1-way ANOVA) (**Fig. 5d,e**), similar to the changes with 5'-Del
249 neurons (**Fig. 3b,h**). Altogether, knockdown of wildtype splicing recapitulated cell-type-specific
250 differences in *NRXN1*$^{+/-}$ 5'-Del neurons, causally implicating decreased wildtype *NRXN1*α
251 expression (LOF) as a key driver of opposing cell-type-specific phenotypes.

252 To reverse the LOF, we pursued approaches that could enhance transcription of *NRXN1*α. β-
253 estradiol was recently reported to reverse *NRXN1* LOF neurogenesis deficits in xenopus and
254 human NPC models (*29*). Although the mechanism of rescue remains unknown, chromatin
255 immunoprecipitation with sequencing (ChIP-Seq) in mouse brain tissue identified estrogen
256 receptor alphaα (ERα) binding sites at the *NRXN1* alpha locus (**Extended Data Fig. 9**) (*30*).
257 Consistent with *NRXN1* being a canonical target of ERα, acute treatment with β-estradiol (10nM
258 or 30nM, 3-5 days) significantly increased *NRXN1*α expression in iGLUT neurons (P= 0.0297 by
259 1-way ANOVA) but not in iGABA neurons derived from 5'-Del (1 male, 1 female) and matched
260 controls (1 male and 1 female) (**Fig. 5f**).

261 For *NRXN1 3*'-Del neurons, we reasoned that reducing the expression of the GOF transcript
262 should restore the changes in synaptic transmission for both iGLUT and iGABA neurons. We
263 designed a shRNA against the mutant splice junction overlapping exons 20 and 24, expressed in
264 all 3'-Del unique *NRXN1* alpha and beta isoforms, and achieved targeted knockdown of mutant
265 splice isoforms by 95% in iGLUT, and 25% in iGABA neurons in both donors (Extended Data Fig
266 6). In the donor with most robust knockdown in both iGLUT (90%) and iGABA (37%) neurons,
267 electrophysiological recordings revealed reversal of changes in synaptic transmission. In iGLUT
268 neurons, shRNA MT decreased sEPSC IEI (P= 3.66E-08 by Levene's Test and P= 0.0361) (**Fig.
269 5i,j**) and in iGABA neurons increased sIPSC IEI (P = 4.23E-02 by Levene's Test) (**Fig 5k,l**), as
270 compared to shRNA-SCR. Notably, the IEIs for rescued neurons appeared similar to those for
271 control iGLUT and iGABA neurons (**Fig. 3b,h**).

272 To investigate a more feasible therapeutic approach, we investigated the utility of anti-sense
273 oligonucleotides (ASO), an appealing strategy for their recent clinical use to treat neurological
274 diseases (*31*), on GOF 3'-Del patients. We designed an ASO that targets the mutant splice
275 junction to facilitate a targeted RNAseH1 dependent degradation of mutant isoforms. Acute ASO
276 treatment (1uM, 3-5 days) resulted in 50-60% knockdown of total mutant isoforms in iGLUT (P<
277 0.001 by student's t-test) and iGABA neurons (P= 0.0016 by student's t-test) relative to a non-
278 targeting ASO (**Fig. 5g,n**). Altogether, increased *NRXN1* expression in 5'-Del neurons and

279 knockdown of mutant splicing in 3'-Del neurons can each rescue the opposing cell-type-specific
280 case/control differences in *NRXN1*$^{+/-}$ neurons, implicating *NRXN1*α expression as a key a driver
281 of *NRXN1* mutant phenotypes.

282 **DISCUSSION**

283 *NRXN1*$^{+/-}$ deletions are linked to diverse clinical outcomes, all of which have been associated with
284 excitatory-inhibitory (E:I) imbalance[1,27,30]. Here, we show that *NRXN1* splicing bidirectionally
285 regulates E:I synaptic transmission, with the 5'-Del and 3'-Del patients reducing sEPSCs but
286 increasing sIPSCs in iGLUT and iGABA neurons, respectively. These changes likely play a critical
287 role in altering the E:I balance, a common theme among neuropsychiatric disorders. Using a
288 case/control *NRXN1*$^{+/-}$ cohort as well as isogenic manipulations of the *NRXN1* isoform repertoire,
289 we report distinct phenotypic effects in human iGLUT and iGABA neurons, which predominately
290 manifest in changes in the frequency of synaptic transmission. These results suggest causal
291 relationships between aberrant splicing and synaptic dysfunction, dictated by unique patient-
292 specific mechanisms. A recent report evaluated the impact of *NRXN1*$^{+/-}$ on forebrain organoids by
293 single cell transcriptomic characterization over time, and highlighted specific perturbations in the
294 developmental trajectories of early neural progenitors (*32*). Likewise, we report divergent
295 proliferation dynamics, with an increase in glutamatergic enriched hCOs, but a decrease in
296 GABAergic-enriched hSOs. While it is mechanistically unclear how mutations in *NRXN1* impact
297 neurogenesis, prior evidence also exists for this phenomenon (*29, 33*), altogether suggesting
298 roles for *NRXN1* beyond mediating synaptic organization and transmission, perhaps similar to
299 *SYNGAP1* (*34*), a gene canonically thought to have exclusive synaptic function. Nevertheless,
300 our causal demonstration of manipulating *NRXN1* splicing, which resulted in the recreation/rescue
301 of synaptic phenotypes in post-mitotic neurons suggests that direct manipulation of splicing may
302 achieve therapeutic benefit in cases.

303 Neurexins are expressed across all synapses and among certain non-neuronal cell-types, such
304 as astrocytes, which may confer distinct functional roles (*35*). With respect to GOF mechanisms,
305 it remains unclear whether mutant isoforms shift the stoichiometry of alternative splicing against
306 wildtype RNA isoforms or alter trans-synaptic protein-protein interactions. Unique patterns of
307 aberrant splicing amongst non-recurrent mutations would be challenging to target with a common
308 pharmacological agent for all *NRXN1*$^{+/-}$ carriers. Given that *NRXN1* fundamentally encodes for
309 pre-synaptic cell adhesion molecules, traditional neuropharmacological agents that target specific
310 receptors within single neurotransmission systems would be unlikely to broadly ameliorate the

311 many levels of neural circuitry impacted across neurodevelopment. Instead, precision therapies
312 that target aberrant splicing are needed to effectively reverse defects in the multiple cell types
313 affected by patient-specific deletions.

314 Our results show that the opposing effects of *NRXN1*$^{+/-}$ in glutamate and GABA neurons provides
315 the foundation for evaluating proof-of-concept therapeutics that target aberrant splicing, once the
316 LOF or GOF phenotype has been determined. We find that ASOs designed to target the mutant
317 splice junction and facilitate degradation of mutant isoforms provides a therapeutic approach to
318 ameliorate the toxic effects of GOF mutations. While gene therapy in brain disease has resulted
319 in mixed successes (*36*), cases of muscular dystrophies which have been treated via splicing
320 modulating ASOs have proved effective (*37*). For LOF mutations, mechanisms for upregulating
321 wild-type allele are needed. Applying steroid-based pharmaceuticals for treating LOF mutations
322 is also feasible, as they have been used to treat neuroinflammation-related conditions (*38*), with
323 recent studies revealing estrogen-mediated roles in neuroprotection (*29*), demonstrating the
324 safety and feasibility of this approach. Altogether, precision medicine provides therapeutic
325 promise for treating neuropsychiatric conditions.

326 Our findings with estrogen-dependent regulation of *NRXN1* expression also hint at possible
327 mechanistic explanations for the dramatic sex differences in the prevalence and severity of autism
328 spectrum disorders, for which the biological basis for the prominent male bias in diagnosis is
329 unknown (*39*). At the genetic level, evidence exists for a female protective effect – the observation
330 that females have a higher threshold for reaching affectation status and require greater mutational
331 burden to express ASD phenotypes due to female-specific protective factors that lead to
332 resilience (*40, 41*). Estradiol ameliorates neurodevelopmental phenotypes in *Xenopus* and
333 zebrafish genetic models of ASD (*29, 42*), suggesting that estradiol might be modulating relevant
334 circuits in the setting of ASD risk genes to mitigate a range of ASD gene mutations. Estradiol
335 modulates excitatory and inhibitory circuits in the developing brain, regulating the switch from
336 excitatory to inhibitory GABAergic signaling in the hippocampus and playing a neuroprotective
337 role against glutamate-induced excitotoxicity (*43, 44*). Consistent with our findings with *NRXN1* in
338 human neurons, estrogens may modulate neurodevelopment at the cellular and circuit levels,
339 conferring resilience in ASDs.

340 While our work carefully considers the cell-type specific impact of *NRXN1* splicing on non-
341 recurrent deletions, it is important to acknowledge certain limitations inherent in our study.
342 Notably, the neuronal subtypes that are yielded from lineage conversion can be diverse and

343 immature, as recently characterized (*45*). Furthermore, the impact of *NRXN1*$^{+/-}$ on synaptic
344 physiology across different subtypes of neurons (e.g., SST versus PV expressing GABA
345 neurons), remains to be determined. Future studies will need to comprehensively assess the
346 impact of *NRXN1*$^{+/-}$ across more discrete cell types and complex multicellular systems.
347 Furthermore, it will be important to also probe the biochemical and proteomic interactions of
348 *NRXN1*. Unbiased proximity-labelling methods such as BioID (*46*), could provide mechanistic
349 insights into *NRXN1* medicated synapse function, by defining alternations in binding profiles from
350 wildtype and mutant isoforms.

351 Based on our strategy of manipulating splicing as a therapeutic strategy for specific *NRXN1*
352 mutations, a similar approach could be applied to loss- and gain-of-function mechanisms linked
353 to mutations in other neuropsychiatric disorder-related synaptic genes (e.g.,
354 *NLGN3* (*47*), *CACNA1D* (*48*), *CACNA1C (49), SCN2A* (*50*)). Taken together, our work
355 highlights important implications for precision medicine treatments of neuropsychiatric disorders,
356 demonstrating the necessity of functionally dissecting the phenotypic impact of diverse patient-
357 specific genetic variants across cellular contexts, to resolve candidate therapies across stratified
358 disease mechanisms.

359

360 **METHODS**

361 *Plasmid designs and molecular cloning*

362 *i. TetO-Ascl1-Neo*

363 The *ASCL1* insert from TetO-Ascl1-Puro (Addgene #97329) was synthesized as a gBLOCK
364 flanked by EcoR1 cut sites, and cloned into TetO-hNgn2-Neo using EcoR1 to remove *NGN2.* The
365 recipient vector was dephosphorylated with shrimp alkaline phosphatase (rSAP NEB #M0371S)
366 during the digest, column purified and ligated at a 1:1 vector to insert ratio using the QuickLig Kit
367 (NEB #M2200S). The *ASCL1* stop codon was subsequently mutated using the QuickChange II-
368 XL site-directed mutagenesis kit (Agilent #200523) and verified via whole plasmid sequencing
369 from plasmidsaurus.

370 *ii. shRNA RNA interference constructs*

371 All shRNAs were designed and produced by Sigma-Aldrich via custom submitted sequences

372 against wildtype *NRXN1α* (constitutively expressed exon 9) and mutant *NRXN1α* (mutant 20/24
373 splice junction) cloned into TCR2 pLKO.5-puro.

374 <u>*Cell Culture*</u>

375 *i. hiPSC culture*

376 Passage matched (±3) human induced pluripotent stem cells (hiPSCs) were cultured in StemFlex
377 media (Life technologies #A3349401) on Matrigel (Corning, #354230). At ~70-80% hiPSCs were
378 clump passaged using 0.5mM EDTA in PBS without Mg/Ca (Life technologies #10010-031). Cells
379 were washed once and incubated for 4-7 min with EDTA at RT. The EDTA was aspirated, and
380 the remaining colonies were lifted off with 1mL of StemFlex and re-distributed at varying densities
381 in a 6–well maintenance plate. hiPSC lines were split every 4-6 days. For neuronal/organoid
382 differentiation, wells of similar confluence across all hiPSC donors were resuspended and seeded
383 onto a Matrigel coated 10cm dish and expanded until ~70-80% confluency.

384 *ii. HEK293T culture and lenti-viral production*

385 HEK293T cells were maintained in 15cm dishes and cultured in DMEM supplemented with 10%
386 standard FBS (Life technologies #16000069). 3rd Gen lenti-viral particles were produced using
387 previously described methods and REV, MDL and VSV-G plasmid ratios (Man-Ho et al., 2015),
388 each transfected with PEImax (Polysciences #24765-1). Each PEIMax batch was volumetrically
389 titrated at total ugDNA:uLPEI for optimal transfection efficiency.

390 *iii. Primary mouse glia production*

391 All mouse work was performed under approved IACUC protocols at the Icahn School of Medicine
392 at Mount Sinai. C57BL/6 mice were used as breeding pairs. For glial preps, dissected cortices
393 from 3 pups (at p0-3) were dissociated using papain (R&D #LS003126) and plated on 10cm
394 dishes in MEF medium (DMEM, 10% Cosmic Calf Serum (Fisher #SH3008703HI), 1x Antibiotic-
395 antimycotic (Life technologies #15240), 1x Sodium Pyruvate (Life technologies #11360070), 1x
396 MEM Non-Essential Amino Acids Solution (Life technologies #11140050), 4uL 2-Mercaptoethanol
397 (Sigma #60-24-2), supplemented with 100µg/mL Normocin (InvivoGen #ant-nr-2). Glial cells were
398 recovered and propagated for 7 days, expanded into three 10cm dishes and were used for co-
399 culture experiments. All glial preps were tested twice for mycoplasma (Normocin withdrawn)
400 (Lonza, #LT07-318) prior to freezing or neuronal co-culture. At day 14, one 10cm dish with mouse
401 glia were distributed to two MEA, 12- or 24- well plates, and subsequently inactivated with 4µM

402 Ara-C (Sigma #C1768) prior to or during re-seeding of induced neurons.

403 *iv. iGLUT induction and astrocyte co-culture*

404 At day -1 hiPSCs expanded in 10cm dishes were dissociated with accutase (StemCell
405 Technologies, #07920), washed and pelleted with a 1:4 ratio of accutase to DMEM for 5 min at
406 1000 rcf, and re-suspended with StemFlex media containing ROCK inhibitor, THX (10μM/mL;
407 Sigma Aldrich, SML1045). The hiPSCs are then co-transduced with TetO-Ngn2-Puro (Addgene
408 #79049) or TetO-Ngn2-Neo (Addgene# 99378) and UCb-rtTA (legacy vector from the lab of Fred
409 Gage) and seeded at 1.0-1.5x10^6 cells in 1.5mL per well on 6-well plates were coated with 2x
410 Matrigel for at least one hour at 37C. The hiPSC-viral mixture was then incubated overnight. The
411 following morning (day 0), a full media change with iGLUT induction media was performed with
412 the following recipe: Neurobasal Media: 1x N2 (Life technologies #17502-048), 1x B-27 minus
413 Vitamin A (Life technologies #12587-010), 1x Antibiotic-Antimycotic, 1x Sodium Pyruvate, 1x
414 GlutaMax (Life technologies #35050), 500μg/mL cyclic-AMP (Sigma #D0627), 200nM L-ascorbic
415 acid (Sigma #A0278), 20ng/ml BDNF (Peprotech #450-02), 20ng/ml GDNF (Peprotech #450-10),
416 1μg/ml natural mouse laminin (Life technologies #23017015). On days 1-2, iGLUT cells were
417 treated with respective antibiotic concentrations at 1ug/mL puromycin (Sigma# P7255) or
418 0.5ug/mL neomycin (Life technologies #11811-031). On day 3, antibiotic medium was withdrawn
419 and iGLUT cells were treated with 4μM Ara-C. On Day 4, iGLUT cells were dissociated with
420 accutase for 15 min, washed and pelleted with a 1:4 ratio of accutase to DMEM for 5 min at 800
421 rcf, and re-suspended with iGLUT media containing ROCK inhibitor, Ara-C and 2% low-
422 hemoglobin FBS (R&D systems #S11510). iGLUT neurons were distributed among wells (500-
423 750k cells per 24wp or 0.75-1.5E6 cell per 12wp) pre-seeded with confluent mouse glia. The
424 following day, iGLUT neurons received a full media change with Brainphys maturation media
425 (Neurobasal Media, 1x N2, 1x B-27 minus Vitamin A, 1x Antibiotic-Antimycotic, 500μg/mL cyclic-
426 AMP, 200nM Ascorbic Acid, 20ng/ml BDNF, 20ng/ml GDNF, 2% low-hemoglobin FBS, 1μg/ml
427 Mouse Laminin) supplemented with Ara-C and were subsequently monitored for growth of non-
428 neuronal/glial cells. Ara-C treatment was tittered down with half-media changes (without Ara-C)
429 every 3-4 days until used for experiments.

430 *v. iGABA induction and astrocyte co-culture*

431 iGABA production paralleled the methods aforementioned. hiPSCs were instead co-transduced
432 with TetO-Ascl1-puro (Addgene #97330) or TetO-Ascl1-neo (Addgene #TBD), TetO-Dlx2-hygro

433 (Addgene #97329) and UCb-rtTA and seeded at 0.8-1.2x10^6 cells in 1.5mL per well on 6-well
434 plates similarly prepared. The following morning (day 0), a full media change with iGABA induction
435 media (DMEM/F-12 + Glutamax, 1x N2, 1x B-27 minus Vitamin A, 1x Antibiotic-Antimycotic) was
436 performed. On days 1-2 iGABA cells were selected with respective antibiotic concentrations at
437 1µg/mL puromycin or 0.5ug/mL neomycin and 0.25ug/mL hygromycin (Life Technologies
438 #10687010), followed by antibiotic withdrawal and Ara-C treatment on day 3. iGABA neurons
439 were re-seeded identically to iGLUT cells, at 150-250k cells per 24wp well. iGABA cultures were
440 morphologically QC'ed prior to all experiments, with uncharacteristic batches being discarded.

441 *vi. Cortical and subpallial organoid differentiation*

442 Cortical organoids were generated according to the protocol described by Sloan et. al. (*51*), with
443 several modifications. hiPSCs were first aggregated into embryoid bodies (EBs) using an
444 AggreWell™800 Microwell Culture Plate system (Stemcell Tech #34850). Expanded hiPSCs
445 were rinsed twice with DPBS without Ca/Mg, and then dissociated using accutase. 3x10E6
446 hiPSCs were added to a single well in the prepared AggreWell and allowed to aggregate in a 37
447 °C incubator for 24 hours. The following day (day 0), EBs were dislodged from the AggreWell
448 plate using a cut p1000 pipette tip and passed over a 40µm strainer, and washed with excess
449 DMEM. The strainer was inverted over an Ultra-Low Attachment 10 cm culture dish and the EBs
450 were collected in spheroid induction media, which contained Stemflex supplemented with two
451 SMAD inhibitors, SB-431542 (SB) and LDN193189 (LDN), and THX. The following day (day 1),
452 the media THX was withdrawn. From d2-d6, induction media was replaced daily, and no longer
453 contained the Stemflex supplement (only base Stemflex media with SB and LDN). On day 6, the
454 media was replaced with organoid patterning media, formulated with Neurobasal-A medium, 1x
455 B-27 minus Vitamin A, 1x GlutaMAX, and 1x Antibiotic-Antimycotic. From d6-d24, organoid
456 maturation media was supplemented with 20 ng/ml of EGF (R&D Systems, #236-EG) and 20
457 ng/ml FGF2 (R&D Systems, #233-FB-01M). Media was changed every day from d6 – d15, after
458 which media was changed every other day. From d25-d43, the organoid maturation media was
459 supplemented with 20 ng/ml of NT-3 (PeproTech, #450-03) and 20 ng/ml BDNF. From d43
460 onwards, organoids received organoid maturation media with no supplements, and media was
461 changed every 4 days or as needed. Subpallial organoids were generated in the same way as
462 cortical organoids, but with additions in media formulations. From d4-d23, hSOs received
463 spheroid induction media or organoid maturation media supplemented with 5 µM of the Wnt
464 inhibitor, IWP-2 (Selleckchem, #S7085). From d12-d23, hSO organoids received neuronal
465 differentiation media supplemented with 100 nM of the SHH agonist, SAG (Selleckchem,

466 #S7779).

467 <u>*Electrophysiology*</u>

468 *i. Multi-electrode array (MEA)*

469 The Axion Maestro (Middleman) system was used to perform all MEA recordings. Measurements
470 began as early as DIV9 for both iGLUT and iGABA co-cultures. For time course experiments,
471 MEA plates were recorded every 2-3 days per week with a full media change prior to each
472 recording.

473 *ii. Whole-cell patch-clamp electrophysiology*

474 For whole-cell patch-clamp recordings, iGLUT or iGABA human-mouse glia co-cultures were
475 recorded at 4-6 weeks following dox-induction (time points specified in figure legends), with a full
476 media change one day prior to recording. Cells were visualized on a Nikon inverted microscope
477 equipped with fluorescence and Hoffman optics. Neurons were recorded with an Axopatch 200B
478 amplifier (Molecular Devices), digitized at 10 kHz using a Digidata 1320a (Molecular Devices) and
479 filtered between 1-10 kHz, using Clampex 10 software (Molecular Devices). Patch pipettes were
480 pulled from borosilicate glass electrodes (Warner Instruments) to a final tip resistance of 3-5 MΩ
481 using a vertical gravity puller (Narishige). Neurons were recorded in Brainphys medium (external
482 solution) with an internal patch solution containing (in mM): K-d-gluconate, 140; NaCl, 4; MgCl2,
483 2; EGTA, 1.1; HEPES, 5; Na2ATP, 2; sodium creatine phosphate, 5; Na3GTP, 0.6, at a pH of 7.4.
484 Osmolarity was 290-295 mOsm. Neurons were chosen at random using DIC and all recordings
485 were made at room temperature (~22°C). Current-clamp measurement occurred across -10pA to
486 +50pA steps, with a maximum stimulus of +60pA, whereas voltage-clamp measurements
487 occurred across -50mV to +50mV steps, normalized to cell capacitance (to control for variable
488 neuronal size). For sEPSC/sIPSC recordings, the internal solution was replaced with (in mM):
489 Cesium-Chloride, 135; HEPES-CoOH, 10; QX-314, 5; EGTA, 5. Osmolarity was 290-295 mOsm.
490 All mEPSC measurements were recorded under the presence of 100nM TTX-citrate (Tocris Cat#
491 1069). mIPSC measurements were made using 100nM TTX-citrate and CNQX-disodium salt
492 (Tocris Cat#1045/1) to pharmacologically inhibit ionotropic glutamate receptors. All chemicals
493 were purchased from Sigma-Aldrich Co. (St. Louis, MO). All toxic compounds were handled in
494 accordance with ISMMS EHS standards.

495 *iii. Patch-clamp data analysis*

496 All patch-clamp data were analyzed on Clampfit (v) and Easy-Electrophysiology (v2.4.1 or beta-
497 versions). Briefly, for voltage-clamp data, files were opened in Easy-Electrophysiology and two
498 bins were assigned for Na+/K+ measures for minimum and maximum current values, respectively.
499 For current-clamp data, files were opened in Easy-Electrophysiology and action potential (AP)
500 analysis was used to automatically determine spike number and properties. For gap-free
501 recordings, all data was post-hoc adjusted to a baseline of zero on ClampFit, and subsequently
502 analyzed in Easy-Electrophysiology by template and linear threshold detection. For case control
503 experiments, a minimum cutoff of 10 events for the duration of the recording (3min) was used as
504 QC. For typical EPSC events, a single template from a randomly chosen recording was used to
505 analyze all traces (with a 30ms decay cutoff). For IPSC events, three templates were used to
506 detect variable GABA receptor kinetics, for all traces (with a 60ms decay cutoff). An amplitude cut
507 off of 7pA was used to call positive events. For cumulative probabilities, each cell was binned by
508 experiment and averaged across all cells for a representative curve (GraphPad Prism v).

509 *RNA-Sequencing and bioinformatic analyses*

510 *i. Bulk RNA sequencing and DEG analysis of iGLUT and iGABA neurons*

511 iGLUT (DIV21) and iGABA (DIV14 or DIV35) co-cultured with primary mouse glia (to match
512 functional experiments) were harvested in Trizol and submitted to the New York Genome
513 Center (*52*) for high-throughput RNA extraction and quality control, library prep using the Kapa
514 Hyper library prep with ribo-erase (Roche #KK8541) and subsequently sequenced on Illumina
515 NovaSeq. Returned raw data files were first processed to remove mouse reads in the RNA-seq
516 data, a combined genome reference (hg38 and mm10) was created using the "mkref" command
517 in cellranger v6.1.2. The raw sequencing reads were then aligned to the combined genome
518 reference using STAR v2.7.2a (*53*). Reads that mapped specifically to the human reference
519 genome were extracted from the resulting BAM files for subsequent gene expression analysis.
520 Gene-level read counts were obtained using the Subread v2.0.1 package featureCount (*54*), and
521 RPKM values were calculated using the R package edgeR (*55*). To confirm sample identity,
522 variants were called from RNA-seq bam files by HaplotypeCaller and GenotypeGVCFs in GATK
523 v4.2.0.0. Then bcftools v1.15 was used to examine variants concordance with variants from
524 whole-exome sequencing data from the same donor. Following donor identity confirmation, the
525 differential gene expression analysis followed the methods as described previously (*56*). First,
526 CibersortX (*57*) was utilized to predict differences in cell type composition across all samples. The
527 R package variancePartition v1.30.2 (*58*) was then employed to investigate the contribution of

528 specific variables to the variance in gene expression. The limma/voom package (*59*) was used
529 for differential expression analysis, with the regression of fibroblast and hiPSC cell type
530 compositions. The analysis began with a comparison between the case and control groups.
531 Subsequently, within each case vs control group, subgroup comparisons were conducted for all
532 four pairs (two donors each for 3'-Del and 5-Del patients and two healthy controls) of samples,
533 accounting for heterogeneity between different donors. Genes with a fold change larger than 1.5
534 between the patient and control group, an FDR less than 0.1, and a fold change larger than 1.5
535 in all four pairs of subgroup comparisons were defined as the final set of differentially expressed
536 genes. Kallisto v0.46.1 (*60*) was used to calculate the *NRXN1* exon usage ratios.

537 *ii. Network Analysis of top DEGs overlapping with disease risk genes*

538 The ASD, BP, and SCZ risk gene lists were extracted from previously curated gene lists (*20*),
539 Genes with the top 200 smallest FDR values and a fold change larger than 1.5 in the case vs
540 control comparison were selected for the protein interaction network analysis. Then, overlapping
541 genes between the selected gene list, the disease risk gene sets, and the proteins in the SIGNOR
542 database (*21*) were utilized to query the SIGNOR database and build the interaction network,
543 using the "connect + add bridge proteins" search mode in The SIGNOR Cytoscape App v1.2. (*61*)

544 *iii. Dissociation and 10x Single-Cell RNA sequencing of organoids*

545 Whole organoids were dissociated to the single cell level in preparation for single-cell RNA
546 sequencing using the Papain Worthington Kit (Worthington, LK003150). All solutions included in
547 the kit were prepared according to the manufacturer's instructions. 4-6 organoids were transferred
548 to one well of a low attachment 6 well plate and were washed with PBS without Ca^{2+} and Mg^{2+}.
549 Organoids were cut with a small scalpel into smaller pieces for easier dissociation. 800 µl of
550 papain solution (supplied in the kit) was added per well. Samples were incubated at 37°C for
551 about two hours or until single cell suspension was achieved. Every 15 minutes, the mixture was
552 pipetted up and down with a cut P1000 pipette tip. Once single cell suspension was reached, 500
553 µl of inhibitor solution (supplied in the kit) was added to the well. The solution was gently mixed,
554 filtered through a 70 µm-pore sieve, and transferred to a 15 ml centrifuge tube. The cells were
555 pelleted by centrifugation at 300 x g for 5 minutes at room temperature. Cell pellets were
556 resuspended in 500 µl of ice-cold 0.04% BSA diluted in PBS without Ca^{2+} and Mg^{2+}. scRNA-seq
557 was performed on 4-6 pooled 6-month-old organoids per donor line, per condition (hCS or hSS)
558 for a total of 48 organoids. A minimum of 10,000 dissociated cells were submitted for sequencing.

559 The library was prepared using the Chromium platform (10x Genomics) with the 3' gene
560 expression (3' GEX) V3/V3.1 kit. Libraries were sequenced on an Illumina NovaSeq sequencer
561 with an S4 flow cell, targeting a minimum depth of 20,000 reads per cell. The lengths for read
562 parameters Read 1, i7 index, i5 index, and Read 2 were 100, 8, 0, 100, respectively.

563 *iv. Bioinformatic analysis of scRNASeq data*

564 The raw sequencing data, represented as base call (BCL) files produced by the Illumina
565 sequencing platform, were subjected to demultiplexing and subsequent conversion into FASTQ
566 format using CellRanger software (version 6.0.0, 10x Genomics) with default parameters. The
567 software then mapped the FASTQ reads to the human reference genome (GRCh38) with default
568 parameters. Following this, the 'count' command in the Cell Ranger v6.0.0 software was utilized
569 for the quantification of gene expression. For alignment and counting, the reference genome
570 refdata-gex-GRCh38-2020-A was used, which was procured from the official 10x Genomics
571 website. We performed QC and normalization using the Seurat v3 R package (*62*). For QC, we
572 filtered out low-quality cells using the following criteria: (i) cells with unique gene counts outside
573 the range of 200 to 6000; (ii) cells with more than 30% mitochondrial gene content; and (*63*) cells
574 with less than 2000 unique molecular identifiers (*64*). Post QC, we carried out normalization,
575 scaling the gene expression measurements for each cell by the total expression, multiplied by a
576 scale factor (10,000 by default), and log-transformed the results. We extracted the expression
577 profiles of the 338 genes identified by Birrey et al (*26*), to reduce the dimensionality of the dataset
578 through principal component analysis (PCA), and identify statistically significant PCs using a
579 JackStraw permutation test. This was followed by non-linear dimensional reduction using the
580 UMAP (Uniform Manifold Approximation and Projection) technique for visualization. Cells were
581 clustered based on their PCA scores using the Shared Nearest Neighbor (SNN) modularity
582 optimization-based clustering algorithm in Seurat. After dimensionality reduction, we used known
583 marker genes to guide the clustering of cells. Each cluster was then annotated using cell type
584 markers identified by Birey et al (*26*). Finally, we conducted differential expression analysis across
585 the defined cell clusters using the FindAllMarkers function in Seurat, which employs a Wilcoxon
586 Rank-Sum test. The significantly differentially expressed genes were then used to interpret the
587 biological significance of cell clusters. For each identified cell type, we conducted an enrichment
588 analysis using the WebGestalt (WEB-based GEne SeT AnaLysis Toolkit) online tool, with the
589 Human genome (GRCh38) as the reference set, employing a hypergeometric statistical method
590 and the Benjamini & Hochberg method for multiple test adjustment.
591

592 *v. Analysis of ChIP-sequencing data from β-estradiol treated rodent brains.*

593

594 Tracks in bigWig format were downloaded from the GEO dataset GSE144718 (*30*). Two peaks
595 within the *NRXN1* gene region in the mm10 genome were visualized using Spark v2.6.2 (*65*)

596

597 *Therapeutic Treatments of iNeurons*

598 *i. Beta-Estradiol treatment*

599 Beta-Estradiol was reconstituted in DMSO and subsequently diluted in Brainphys maturation
600 media for a final concentration of 10 or 30nM. Neurons were treated for 3-5 consecutive days,
601 with fresh drug or vehicle control replenished daily. iGLUT and iGABA neurons were treated
602 starting from ~DIV14-18. On the final day of treatment, cells were harvested ~4 hours post
603 dosage.

604 *ii. Antisense Oligonucleotide treatment*

605 A single HPLC-grade ASO was designed from Qiagen (LNA GapmeR) against the mutant (Ex
606 20/24) splice junction containing a phosphorothioate modified backbone with or without a 5'-FAM
607 label for fluorescent visualization. All experiments were performed matched with a non-targeting
608 ASO as the control group. ASOs were delivered using Lipofectamine RNAiMAX Transfection
609 Reagent (Thermo, #13778075). The Lipofectamine RNAiMAX was diluted in Opti-MEM Medium
610 (Thermo, #31985070). ASO was then diluted in Opti-MEM Medium. The diluted ASO was added
611 in a 1:1 ratio to the diluted Lipofectamine RNAiMAX and incubated at room temperature for 5
612 minutes. The ASO-lipid complex was added to cells, and incubated for 72 hours post-transfection,
613 until RNA harvest.

614 *Molecular Biology and Imaging*

615 *i. RNA extraction and RT-qPCR*

616 For the isolation of RNA, 2D cells were lysed using TRIzol (Life Technologies #15596026) and
617 purified using the Qiagen miRNeasy Kit (Qiagen Cat# 74106) according to the manufacturer's
618 instructions. For 3D organoids, pooled (early timepoints) or single organoids were washed and
619 lysed using TRIzol, by manual homogenization with a pestle in a 1.5mL centrifuge tube. Following
620 purification, samples were normalized within each experiment (15-50ng) and subsequently used

621 for RT-qPCR assays using the *Power* SYBR Green RNA-to-Ct 1-Step Kit (Thermo REF 4389986).
622 Relative transcript abundance was determined using the ΔΔCT method and normalized to the
623 *ACTB* housekeeping gene. All primer sequences are listed below.

624 shRNA, primers and oligonucleotide probe sequences

Target	Sequences (5'-3')	Supplier
RT-qPCR Primer Probes		
NRXN1 (wildtype) Forward	AGAAAGATGCCAAGCACCCA	ThermoFisher
NRXN1 (wildtype) Reverse	CCCATGTCCAGGAGGAGGTA	ThermoFisher
NRXN1-20/24 (mutant) Forward	GCTACCCTGCAGCCAACC	ThermoFisher
NRXN1-20/24 (mutant) Reverse	GACCATACCCGTGGTGCTG	ThermoFisher
ACTB Forward	TGTCCCCCAACTTGAGATGT	ThermoFisher
ACTB Reverse	TGTGCACTTTTATTCAACTGGTC	ThermoFisher
MAP2 Forward	AAACTGCTCTTCCGCTCAGACACC	ThermoFisher
MAP2 Reverse	GTTCACTTGGGCAGGTCTCCACAA	ThermoFisher
NEUROD1 Forward	GGTGCCTTGCTATTCTAAGACGC	ThermoFisher
NEUROD1 Reverse	GCAAAGCGTCTGAACGAAGGAG	ThermoFisher
SLC17A7 Forward	CGCATCATGTCCACCACCAACGT	ThermoFisher
SLC17A7 Reverse	GAGTAGCCGACCACCAACAGCAG	ThermoFisher
SLC17A6 Forward	TCAACAACAGCACCATCCACCGC	ThermoFisher
SLC17A6 Reverse	GTTTCCGGGTCCCAGTTGAATTTGG	ThermoFisher
GAD65 Forward	CTATGACACTGGAGACAAGGC	ThermoFisher

GAD65 Reverse	CAAACATTTATCAACATGCGCTTC	ThermoFisher
DLX5 Forward	ACAGAGACTTCACGACTCCCAG	ThermoFisher
DLX5 Reverse	TGTGGGGCTGCTCTGGTCTA	ThermoFisher
<u>shRNA Sequences</u>		
NRXN1 wildtype mRNA (Exon 9)	ATGGAGTGGTGGCATTTAAAT	Sigma
NRXN1 mutant mRNA (Overlapping Exon 20/24)	CGCTACCCTGCAGCCAACCCA	Sigma
<u>Antisense Oligonucleotides (LNA Gapmers)</u>		
Non-targeting ASO	AACACGTCTATACGC/36-FAM/	Qiagen
NRXN1-Splice ASO	GGTTGGCTGCAGGGTA/36-FAM/	Qiagen

ii. Bright Field Imaging

For organoid perimeter analyses, brightfield microscope images of organoids were taken with a 2x objective. Image analysis was performed in ImageJ, with best fitting ovals or ellipses were selected around an organoid, and perimeter was measured.

iii. Immunostaining of 2D cultures

For immunostaining of 2D monocultures, iGLUT and iGABA neurons seeded on acid-etched coverslips coated with PEI buffered with boric acid and 4x Matrigel. Samples were washed with DPBS $Ca^{2+/}Mg2^{+}$ and fixed using cold, fresh 16% paraformaldehyde (Life Technologies, #28908), diluted to 4% for 12 minutes at RT. Coverslips were then blocked and permeabilized with 2% donkey serum in DPBS $Ca^{2+/}Mg2^{+}$ supplemented with 0.1% Triton-X (Sigma, #93443-100ML) (blocking buffer), for one hour at RT. Primary antibody solutions were prepared in blocking buffer and incubated overnight at 4°C. The following day, samples were washed three times with PBS, and treated with secondary antibodies diluted in blocking buffer, for 1 hour in a dark chamber. Finally, samples were washed three times, and stained with DAPI for 15min at RT during the final wash. Coverslips were mounted with antifade (Vectashield #H-1000-10) onto glass slides and

641 stored at 4°C until imaging using an upright Zeiss LSM 780 confocal microscope.

642 *iv. Immunostaining 3D cultures*

643 For immunostaining of 3D organoids, samples were first washed with DPBS $Ca^{2+}/Mg2^{+}$ and fixed
644 using cold 4% PFA for 2 hours at 4°C. Organoids were then washed with DPBS $Ca^{2+}/Mg2^{+}$
645 supplemented with 10% sucrose (Sigma, #S0389-500G) for one hour. Sucrose percent was
646 increased to 20% for an additional hour, and finally 30% for an overnight incubation. The following
647 day, upon observing the organoids saturated sunk to the bottom of the 1.5mL tube, organoids
648 were transferred to OCT (Sakura #4583) twice in order to remove residual sucrose solution, and
649 snap frozen in a cryopreservation mold with dry ice and stored at –80°C until cryosectioned.
650 Organoids were sectioned at 20 µm thickness onto a Superfrost *Plus* slide (Fisher Scientific, #22-
651 037-246) and stored at -20°C until immunohistochemistry staining. Boundaries were drawn
652 around tissue sections with a lipid pen (Fisher Scientific, #NC9545623) to contain solution and
653 slides were washed once with DPBS with Ca^{2+}/Mg^{2+} to remove excess OCT compound. Slides
654 were then washed twice with 0.01% Triton-X in DPBS with Ca^{2+}/Mg^{2+} (DPBS-TX) and were
655 blocked in 2% Donkey Serum in DPBS-TX for one hour at RT. Primary antibody incubation
656 mixtures were diluted in 2% Donkey Serum in DPBS-TX (see below for a list of primary and
657 secondary antibodies and dilutions used). 100 µl of primary antibody mixtures was added per
658 slide, and allowed to incubate overnight in a humidified chamber at 4°C. Pieces of parafilm were
659 added on top of primary antibody mixtures to further prevent dehydration of slides. The following
660 day, slides were washed three times with DPBS-TX. Secondary antibodies were diluted in DPBS-
661 TX and were allowed to incubate for an hour. Slides were again washed three times with DPBS-
662 TX. A 1:2000 DAPI solution diluted in DPBS-TX was applied to slides for 10 minutes. Secondary
663 and DAPI stainings took place in a covered chamber in order to minimize exposure to light. Slides
664 were washed twice with DPBS-TX, and then once with DPBS with Ca^{2+} and Mg^{2+}. Slides were
665 mounted with coverslips using Aqua Polymount solution (Polysciences #18606-20). Slides were
666 stored at -20 °C until they were imaged.

Target	Antibody Dilution	Supplier/ CAT#
<u>Primary Antibodies</u>		
MAP2AB	1:500	Sigma, #M1406
(Rabbit) vGAT	1:500	Synaptic Systems, #135-303

(Rabbit) vGLUT1	1:500	Synaptic Systems, #131-002
SOX2	1:200	Santa Cruz Biotechnology, #sc-365964
(Rabbit) KI67	1:300	Abcam, #ab15580
(Chicken) MAP2	1:250	Aves Labs, #MAP
DAPI	1:1000	Sigma, #D9542
<u>Secondary Antibodies</u>		
(Donkey) 488-Mouse	1:200	Jackson ImmunoResearch, # 711-545-152
(Donkey) 568-Rabbit	1:200	Abcam, #ab175700
(Donkey) 647-Chicken	1:200	Jackson ImmunoResearch, # 703-605-155
(Donkey) 568-Mouse	1:500	Invitrogen (A10037)
(Donkey) 488-Rabbit	1:1000	Life Technologies (A-21206)

Data and Code Availability

All source donor hiPSCs have been deposited at the Rutgers University Cell and DNA Repository (study 160; http://www.nimhstemcells.org/) and all bulk and single-cell transcriptome sequencing data are being prepared for deposits to GEO. To facilitate improved reproducibility of our data analyses, custom scripts will be deposited to github post peer-review.

Acknowledgements

MBF is supported by a Gilliam Fellowship from the Howard Hughes Medical Institute. This work is supported by the National Institute of Mental Health grants RO1 MH121074-02 (KJB, GF and PAS) and RO1 MH125579-02 (GF and KJB). We thank the Stem Cell Engineering Core at the Icahn School of Medicine at Mount Sinai. The authors are grateful to the labs of Nan Yang (Ruiqi Hu and Xiaoting Zhou) and Samuele Marro (Madel Durens) for assistance in primary glial

preparations. The authors thank Kayla G. Townsley and Mark G. Baxter for advice on statistical testing. Finally, the authors thank all members of the Brennand, Slesinger and Fang labs for critical feedback and discussions throughout the course of this work.

Author Information

MBF, SK, ANM, RO, CP, AP performed and analyzed experiments supervised by PAS and KJB. YZ and YF performed bioinformatic analyses supervised by GF. SG contributed to RNASeq analyses. SW produced virus for the generation of iGABA neurons. MBF, GF, PAS and KJB wrote the paper with input from all authors.

Ethics declarations / Competing interest statement.

The authors have no competing interests to declare.

Figures

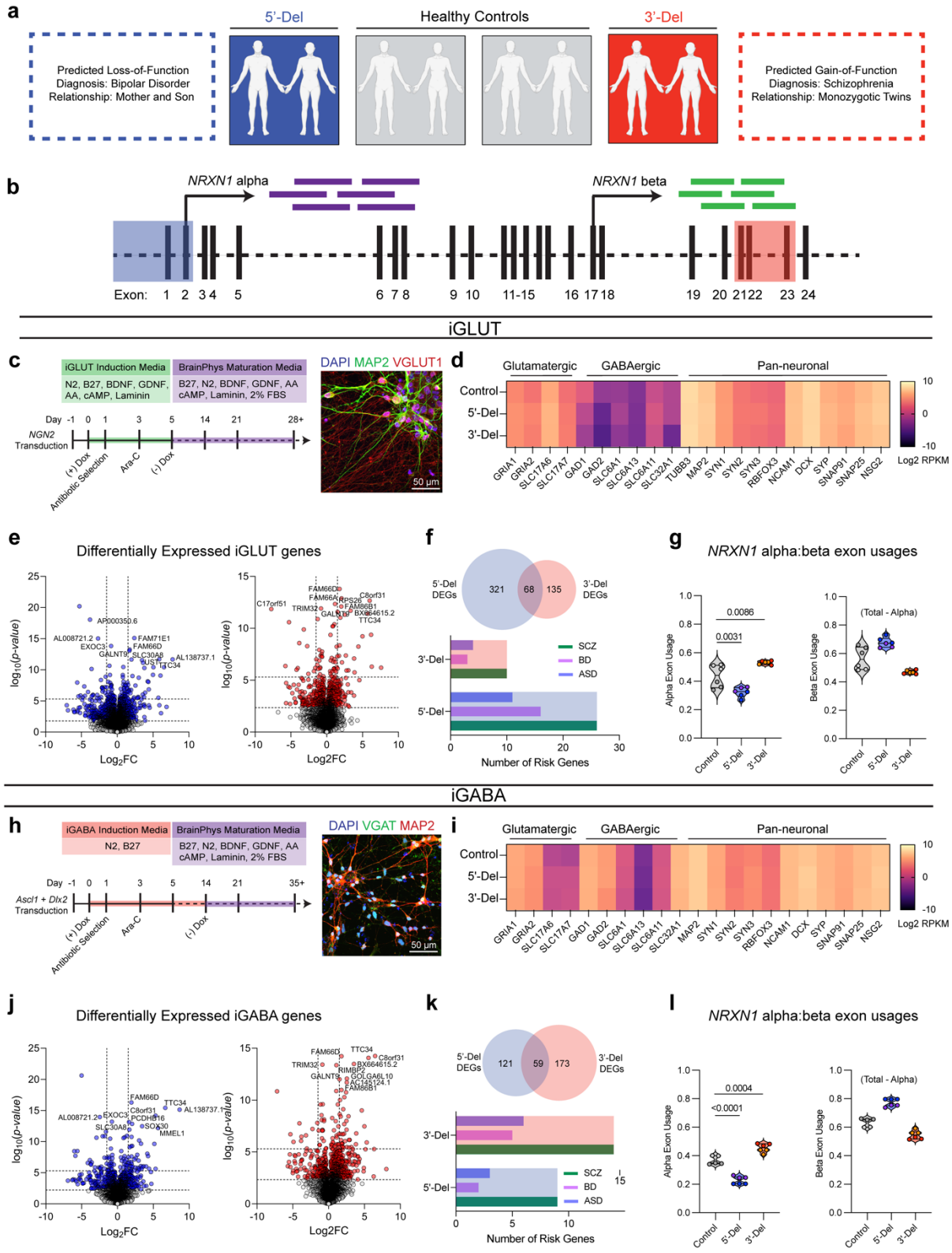
a
5'-Del
Healthy Controls
3'-Del
Predicted Loss-of-Function
Diagnosis: Bipolar Disorder
Relationship: Mother and Son
Predicted Gain-of-Function
Diagnosis: Schizophrenia
Relationship: Monozygotic Twins
b
NRXN1 alpha
NRXN1 beta
Exon: 1 2 3 4 5 6 7 8 9 10 11-15 16 17 18 19 20 21 22 23 24
iGLUT
c
iGLUT Induction Media
N2, B27, BDNF, GDNF, AA, cAMP, Laminin
BrainPhys Maturation Media
B27, N2, BDNF, GDNF, AA cAMP, Laminin, 2% FBS
Day -1 0 1 3 5 14 21 28+
NGN2 Transduction
(+) Dox
Antibiotic Selection
Ara-C
(-) Dox
DAPI MAP2 VGLUT1
50 µm
d
Glutamatergic
GABAergic
Pan-neuronal
Control
5'-Del
3'-Del
GRIA1 GRIA2 SLC17A6 SLC17A7 GAD1 GAD2 SLC6A1 SLC6A13 SLC6A11 SLC32A1 TUBB3 MAP2 SYN1 SYN2 SYN3 RBFOX3 NCAM1 DCX SYP SNAP91 SNAP25 NSG2
Log2 RPKM
e
Differentially Expressed iGLUT genes
log10(p-value)
Log2FC
f
5'-Del DEGs
321
68
135
3'-Del DEGs
SCZ
BD
ASD
Number of Risk Genes
g
NRXN1 alpha:beta exon usages
0.0086
0.0031
Alpha Exon Usage
(Total - Alpha)
Beta Exon Usage
Control
5'-Del
3'-Del
iGABA
h
iGABA Induction Media
N2, B27
BrainPhys Maturation Media
B27, N2, BDNF, GDNF, AA cAMP, Laminin, 2% FBS
Day -1 0 1 3 5 14 21 35+
Ascl1 + Dlx2 Transduction
(+) Dox
Antibiotic Selection
Ara-C
(-) Dox
DAPI VGAT MAP2
50 µm
i
Glutamatergic
GABAergic
Pan-neuronal
Control
5'-Del
3'-Del
Log2 RPKM
j
Differentially Expressed iGABA genes
log10(p-value)
Log2FC
k
5'-Del DEGs
121
59
173
3'-Del DEGs
SCZ
BD
ASD
Number of Risk Genes
l
NRXN1 alpha:beta exon usages
0.0004
<0.0001
Alpha Exon Usage
(Total - Alpha)
Beta Exon Usage
Control
5'-Del
3'-Del

693 **Figure 1.** *Changes in NRXN1 splicing are conserved across human iPSC derived glutamatergic*
694 *(iGLUT) and GABAergic (iGABA) neurons.* (a) Brief description of clinical information of all hiPSC
695 lines used in this study, and (b) schematic of *NRXN1* gene structure with red and blue shades
696 corresponding on 3'-Del and 5'-Del genotypes, respectively. Arrows indicate relative internal
697 promoter positions with purple bars corresponding to alpha exons, and green bars correlating to
698 beta exons. (c, h) Induction timeline and factors to generate iGLUT and iGABA neurons, with
699 immunostaining validation of neuronal identity (MAP2), glutamate identity (vGLUT1), and GABA
700 identity (vGAT). (d, i). Gene expression panel confirming abundance of neuronal markers and
701 neurotransmitter identity (n = 6 donors | 2-3 RNASeq replicates per donor averaged within
702 genotypes). (e, j) Volcano plots of differential gene expression (DE) analysis across both
703 genotypes. Vertical dashed lines represent DE genes above/below 1.5 Log_2FC. Horizontal
704 dashed lines represent FDR = 0.1 cutoff (lower) and Bonferroni corrected cutoff. (f, j) Overlap of
705 DEGs between genotypes and enrichment of genes across neuropsychiatric disorders. (g)
706 Percent usage of alpha *NRXN1* exon usage, compared via a 1-way ANOVA, with Dunnett's test,
707 and (l) beta *NRXN1* exon usage, calculated by subtracting alpha-specific reads against total
708 reads.

709

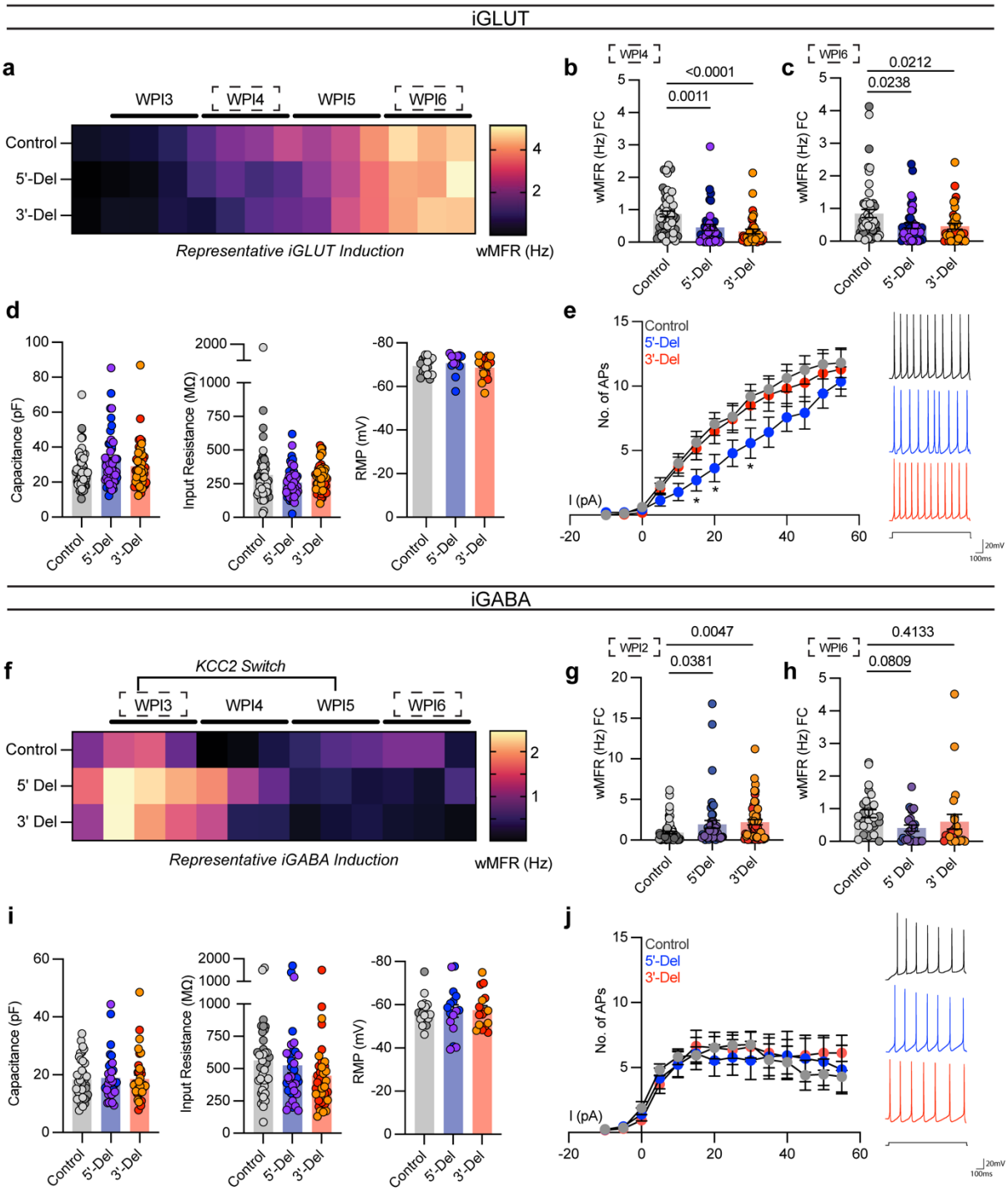

Figure 2. *Spontaneous, passive, and excitable membrane properties are minimally changed in NRXN1$^{+/-}$ induced neurons.* (a, f) Timelapse of multi-electrode array recordings every 2-3 days apart starting near ~DIV12 for a single representative induction. Tiles represent averaged wMFR values across genotypes during a single recording session. (b,c) Quantification of iGLUT neuronal

activity at WPI4 and WPI6; n= 6 donors | 3 inductions | 132 MEA wells. (g, h) iGABA activity at WPI2 (n = 8 donors | 5 inductions | 174 MEA wells), and WPI6 (n= 6 donors | 2 inductions | 73 MEA wells). (d) Passive measures of iGLUT membrane properties: cell capacitance (cm), input resistance (n = 6 donors | 2 inductions | 150 neurons), and membrane resistance (n = 6 donors | 2 inductions | 46 neurons). All p-values = n.s. via 1-way ANOVA, with Dunnett's test. (e) Input-output curves of excitable properties (n = 6 donors | 2 inductions | 36 neurons), with representative traces (right). Genotype effect p-val = n.s. via 2-Way ANOVA, with Dunnett's test. (i) Passive measures of iGABA membrane properties: cell capacitance (cm), input resistance (n = 6 donors | 2 inductions | 110 neurons), and membrane resistance (n = 6 donors | 2 inductions | 50 neurons). All p-values = n.s. via 1-way ANOVA, with Dunnett's test. (j) Input-output curves of excitable properties (n = 6 donors | 3 inductions | 47 neurons), with representative traces (right). Genotype effect p-val = n.s. via 2-Way ANOVA, with Dunnett's test.

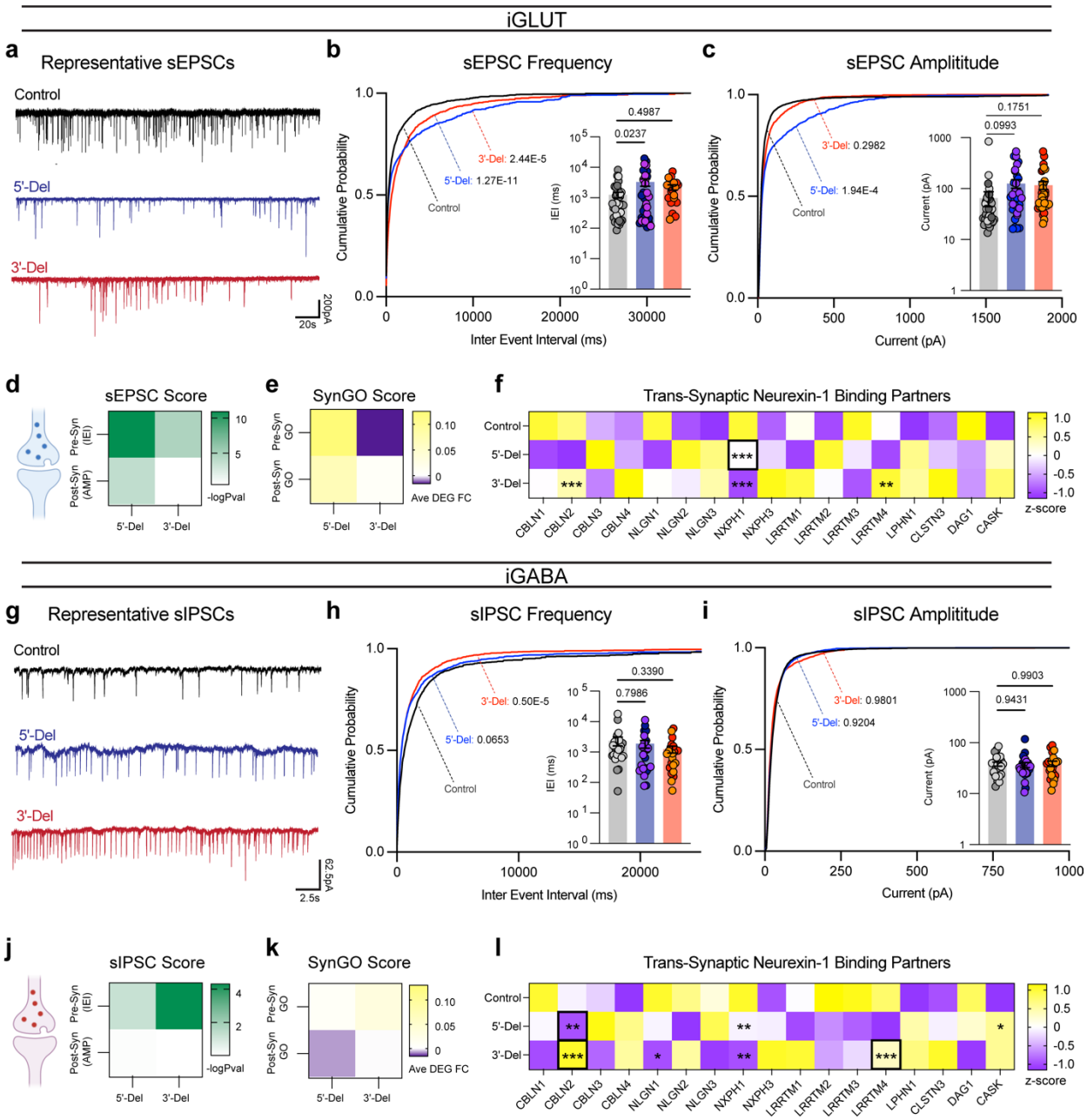

Figure 3: *Divergent impact of NRXN1$^{+/-}$ deletions on neurotransmission in induced neurons.* (a, e) Representative traces of sEPSCs and sIPSCs. (b, h), Cumulative probabilities of inter-event-internals (IEI), across genotypes (Compared by Levene's Test). Inset represent log-scaled IEI (compared by 1-way ANOVA, with Dunnett's test. (c, i), Cumulative probabilities of event amplitudes across genotypes (Compared by Levene's Test). Inset represent log-scaled amplitude (compared by 1-way ANOVA, with Dunnett's test); iGLUT n = 8 donors | 6 inductions | 91 neurons, iGABA n = 6 donors | 4 inductions | 73 neurons. (d, j) Transformed p-values of Levene's Test and

736 (e, k) SynGO gene-set averaged log_2FC values across pre- or post- synaptic genes. (f, l) Gene
737 expression panel (RPKM fold change, relative to control donors), of canonical *NRXN1* binding
738 partners, boxes indicate reaching genome wide significance. $^{*}P < 0.05$, $^{**}P < 0.01$, $^{***}P < 0.001$,
739 Wilcoxon's rank sum test, FDR = 0.05.

740

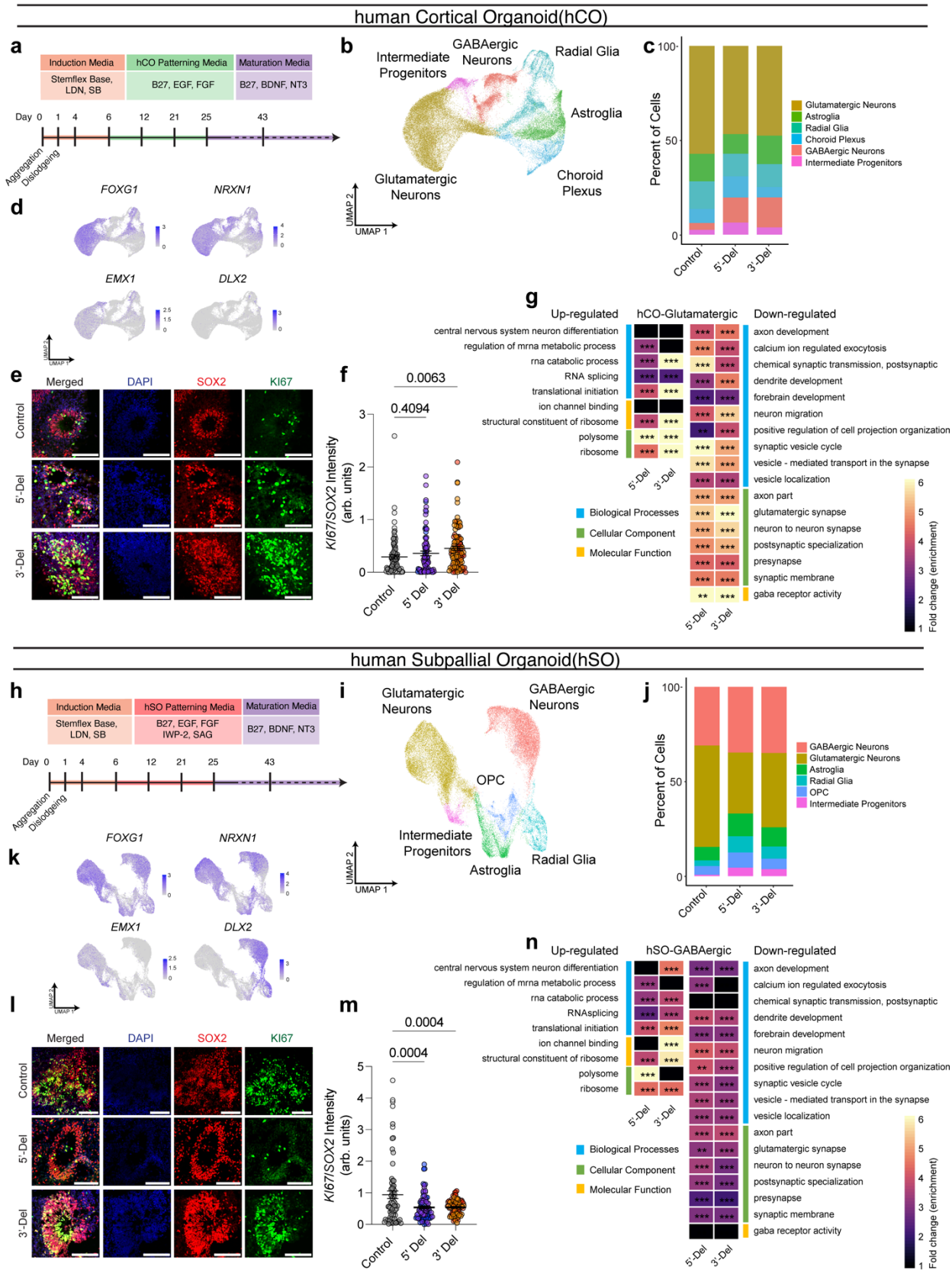
human Cortical Organoid(hCO)
a
Induction Media
Stemflex Base, LDN, SB
hCO Patterning Media
B27, EGF, FGF
Maturation Media
B27, BDNF, NT3
Day 0 1 4 6 12 21 25 43
Aggregation
Dislodgeing
b
Intermediate Progenitors
GABAergic Neurons
Radial Glia
Astroglia
Glutamatergic Neurons
Choroid Plexus
UMAP 2
UMAP 1
c
Percent of Cells
Glutamatergic Neurons
Astroglia
Radial Glia
Choroid Plexus
GABAergic Neurons
Intermediate Progenitors
Control
5'-Del
3'-Del
d
FOXG1
NRXN1
EMX1
DLX2
e
Merged
DAPI
SOX2
KI67
Control
5'-Del
3'-Del
f
0.0063
0.4094
KI67/SOX2 Intensity (arb. units)
Control
5' Del
3' Del
g
Up-regulated
hCO-Glutamatergic
Down-regulated
central nervous system neuron differentiation
regulation of mrna metabolic process
rna catabolic process
RNA splicing
translational initiation
ion channel binding
structural constituent of ribosome
polysome
ribosome
axon development
calcium ion regulated exocytosis
chemical synaptic transmission, postsynaptic
dendrite development
forebrain development
neuron migration
positive regulation of cell projection organization
synaptic vesicle cycle
vesicle - mediated transport in the synapse
vesicle localization
axon part
glutamatergic synapse
neuron to neuron synapse
postsynaptic specialization
presynapse
synaptic membrane
gaba receptor activity
Biological Processes
Cellular Component
Molecular Function
Fold change (enrichment)
human Subpallial Organoid(hSO)
h
Induction Media
Stemflex Base, LDN, SB
hSO Patterning Media
B27, EGF, FGF IWP-2, SAG
Maturation Media
B27, BDNF, NT3
Day 0 1 4 6 12 21 25 43
Aggregation
Dislodgeing
i
Glutamatergic Neurons
GABAergic Neurons
OPC
Intermediate Progenitors
Radial Glia
Astroglia
UMAP 2
UMAP 1
j
Percent of Cells
GABAergic Neurons
Glutamatergic Neurons
Astroglia
Radial Glia
OPC
Intermediate Progenitors
Control
5'-Del
3'-Del
k
FOXG1
NRXN1
EMX1
DLX2
l
Merged
DAPI
SOX2
KI67
Control
5'-Del
3'-Del
m
0.0004
0.0004
KI67/SOX2 Intensity (arb. units)
Control
5' Del
3' Del
n
Up-regulated
hSO-GABAergic
Down-regulated
central nervous system neuron differentiation
regulation of mrna metabolic process
rna catabolic process
RNAsplicing
translational initiation
ion channel binding
structural constituent of ribosome
polysome
ribosome
axon development
calcium ion regulated exocytosis
chemical synaptic transmission, postsynaptic
dendrite development
forebrain development
neuron migration
positive regulation of cell projection organization
synaptic vesicle cycle
vesicle - mediated transport in the synapse
vesicle localization
axon part
glutamatergic synapse
neuron to neuron synapse
postsynaptic specialization
presynapse
synaptic membrane
gaba receptor activity
Biological Processes
Cellular Component
Molecular Function
Fold change (enrichment)

742 **Figure 4:** *NRXN1$^{+/-}$ deletions impact patterning of region-specific human brain organogenesis.*
743 (a, h) Timeline of organogenesis protocols (b, i), UMAPs of human cortical organoid and subpallial
744 organoid (hSO) samples sequenced at 6 months, annotated by cell clusters, and (c, j) relative
745 proportions of cell clusters across genotypes, (hCO = 5 donors | 1 batch | 47,460 cells) and (hSO
746 = 5 donors | 1 batch | 35,563 cells). (d, k) validation of regionalization across forebrain (*FOXG1*),
747 dorsal (*EMX1*) and ventral (*DLX2*) regions, with *NRXN1* expression across all cells. (e, l)
748 Representative images of neural rosettes, immunostained with SOX2, KI67 and DAPI, across
749 genotypes with (f, m) quantified intensity ratios for hCO (n = 6 donors | 2 batches | 284 rosettes
750 from 12 organoids) and hSO (n = 6 donors | 2 batches | 231 rosettes from 10 organoids),
751 compared via 1-way ANOVA, with Dunnett's test. (g, n) Gene ontological analysis results using
752 DEGs from scRNASeq. $^{*}P < 0.05$, $^{**}P < 0.01$, $^{***}P < 0.001$, Wilcoxon's rank sum test, FDR =
753 0.05.

754

755

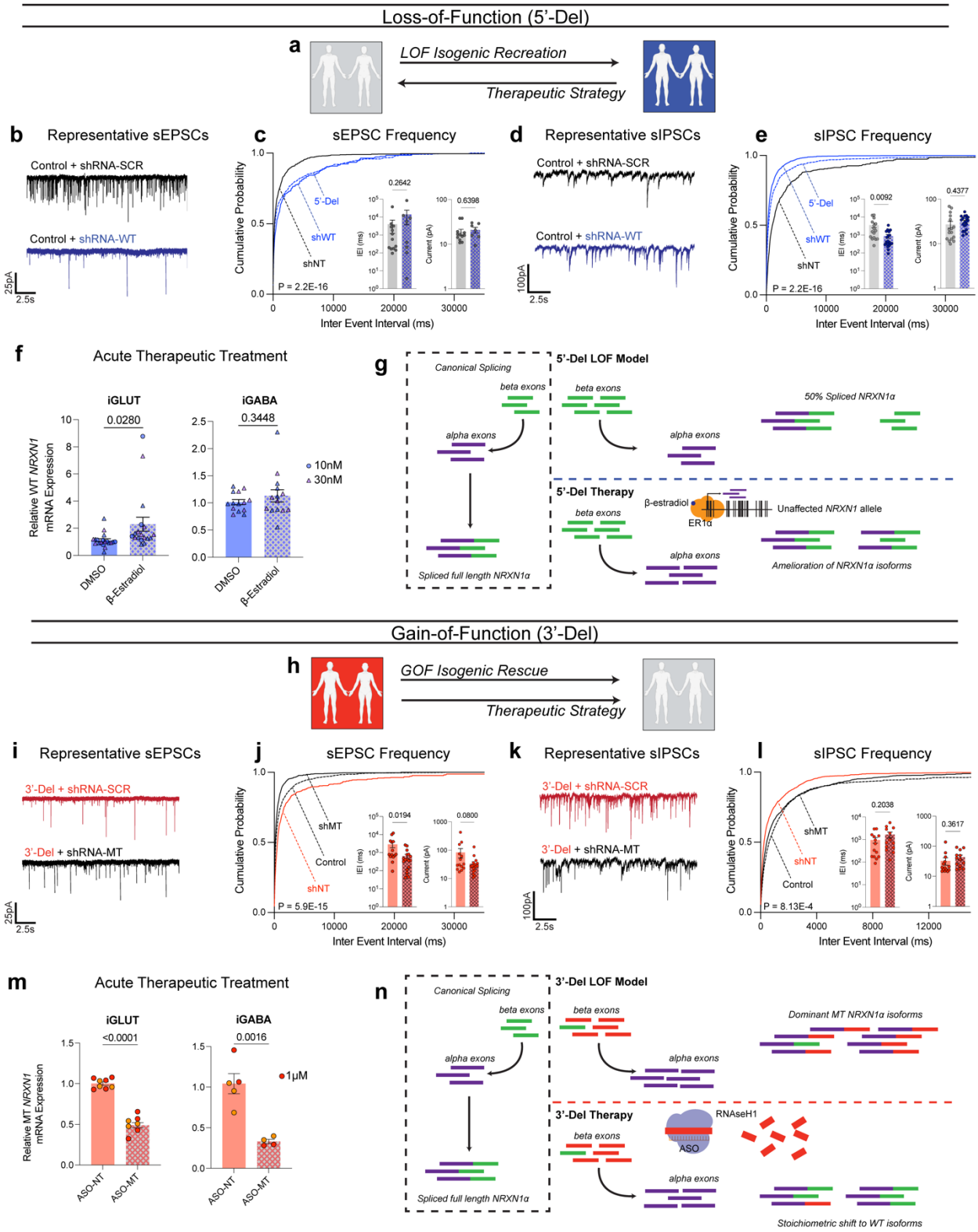

Figure 5: *Isogenic recapitulation and rescue of neurotransmission phenotypes, with strategies for precise therapeutic targeting.* (a, h) Schematic of isogenic and therapeutic strategies

759 (phenotypic recreation or rescue). (b) Representative traces of iGLUT wildtype knockdown
760 effects, with (c) cumulative probabilities of sEPSC kinetics (insets represent log-scaled IEI and
761 amplitude measures). Curves were compared via a Levene's test, and insets were compared via
762 a 1-way ANOVA with Dunnett's test (iGLUT n = 1 isogenic pair | 2 inductions | 19 neurons). (d)
763 Representative traces of iGABA wildtype knockdown effects, with (e) cumulative probabilities of
764 sIPSC kinetics (insets represent log-scaled IEI and amplitude measures). Curves were compared
765 via a Levene's test, and insets were compared via a 1-way ANOVA with Dunnett's test (iGABA n
766 = 3 isogenic pairs | 2 inductions | 35 neurons). (f) Precision β-estradiol treatment of stratified LOF-
767 patients (compared via a student's t-test). (g) Proposed 5'-Del LOF model and mechanism of
768 action. (i) Representative traces of iGLUT mutant knockdown effects, with (j) cumulative
769 probabilities of sEPSC kinetics (insets represent log-scaled IEI and amplitude measures). Curves
770 were compared via a Levene's test, and insets were compared via a 1-way ANOVA with Dunnett's
771 test (iGLUT n = 1 isogenic pair | 2 inductions | 32 neurons). (k) Representative traces of iGABA
772 mutant knockdown effects, with (l) cumulative probabilities of sIPSC kinetics (insets represent
773 log-scaled IEI and amplitude measures). Curves were compared via a Levene's test, and insets
774 were compared via a 1-way ANOVA with Dunnett's test (iGABA n = 1 isogenic pairs | 2 inductions
775 | 27 neurons). (m) Precision ASO treatment of stratified GOF-patients (compared via a student's
776 t-test). (n) Proposed 3'-Del GOF model and mechanism of action.

References

1. T. C. Sudhof, Synaptic Neurexin Complexes: A Molecular Code for the Logic of Neural Circuits. *Cell* **171**, 745-769 (2017).
2. J. de Wit, A. Ghosh, Specification of synaptic connectivity by cell surface interactions. *Nat Rev Neurosci* **17**, 22-35 (2016).
3. X. Yang *et al.*, Widespread Expansion of Protein Interaction Capabilities by Alternative Splicing. *Cell* **164**, 805-817 (2016).
4. D. Schreiner *et al.*, Targeted combinatorial alternative splicing generates brain region-specific repertoires of neurexins. *Neuron* **84**, 386-398 (2014).
5. M. V. Fuccillo *et al.*, Single-Cell mRNA Profiling Reveals Cell-Type-Specific Expression of Neurexin Isoforms. *Neuron* **87**, 326-340 (2015).
6. C. R. Marshall *et al.*, Contribution of copy number variants to schizophrenia from a genome-wide study of 41,321 subjects. *Nat Genet* **49**, 27-35 (2017).
7. N. Matsunami *et al.*, Identification of rare recurrent copy number variants in high-risk autism families and their prevalence in a large ASD population. *PLoS One* **8**, e52239 (2013).
8. R. S. Moller *et al.*, Exon-disrupting deletions of NRXN1 in idiopathic generalized epilepsy. *Epilepsia* **54**, 256-264 (2013).
9. M. S. Ching *et al.*, Deletions of NRXN1 (neurexin-1) predispose to a wide spectrum of developmental disorders. *Am J Med Genet B Neuropsychiatr Genet* **153B**, 937-947 (2010).
10. A. Y. Huang *et al.*, Rare Copy Number Variants in NRXN1 and CNTN6 Increase Risk for Tourette Syndrome. *Neuron* **94**, 1101-1111 e1107 (2017).
11. H. M. Grayton, M. Missler, D. A. Collier, C. Fernandes, Altered social behaviours in neurexin 1alpha knockout mice resemble core symptoms in neurodevelopmental disorders. *PLoS One* **8**, e67114 (2013).
12. C. Pak *et al.*, Human Neuropsychiatric Disease Modeling using Conditional Deletion Reveals Synaptic Transmission Defects Caused by Heterozygous Mutations in NRXN1. *Cell stem cell* **17**, 316-328 (2015).
13. C. Pak *et al.*, Cross-platform validation of neurotransmitter release impairments in schizophrenia patient-derived NRXN1-mutant neurons. *Proc Natl Acad Sci U S A* **118**, (2021).

809 14. E. Flaherty *et al.*, Neuronal impact of patient-specific aberrant NRXN1alpha splicing. *Nat*
810 *Genet* **51**, 1679-1690 (2019).
811 15. S. M. Ho *et al.*, Rapid Ngn2-induction of excitatory neurons from hiPSC-derived neural
812 progenitor cells. *Methods* **101**, 113-124 (2016).
813 16. N. Barretto *et al.*, ASCL1- and DLX2-induced GABAergic neurons from hiPSC-derived
814 NPCs. *J Neurosci Methods* **334**, 108548 (2020).
815 17. Y. Zhang *et al.*, Rapid single-step induction of functional neurons from human pluripotent
816 stem cells. *Neuron* **78**, 785-798 (2013).
817 18. N. Schrode *et al.*, Synergistic effects of common schizophrenia risk variants. *Nat Genet*
818 **51**, 1475-1485 (2019).
819 19. N. Yang *et al.*, Generation of pure GABAergic neurons by transcription factor
820 programming. *Nat Methods*, (2017).
821 20. C. Seah *et al.*, Modeling gene x environment interactions in PTSD using human neurons
822 reveals diagnosis-specific glucocorticoid-induced gene expression. *Nat Neurosci* **25**,
823 1434-1445 (2022).
824 21. P. Lo Surdo *et al.*, SIGNOR 3.0, the SIGnaling network open resource 3.0: 2022 update.
825 *Nucleic Acids Res* **51**, D631-d637 (2023).
826 22. M. A. Virtanen, P. Uvarov, M. Mavrovic, J. C. Poncer, K. Kaila, The Multifaceted Roles of
827 KCC2 in Cortical Development. *Trends in neurosciences* **44**, 378-392 (2021).
828 23. A. M. Gomez, L. Traunmüller, P. Scheiffele, Neurexins: molecular codes for shaping
829 neuronal synapses. *Nature Reviews Neuroscience* **22**, 137-151 (2021).
830 24. V. S. Sohal, J. L. R. Rubenstein, Excitation-inhibition balance as a framework for
831 investigating mechanisms in neuropsychiatric disorders. *Mol Psychiatry* **24**, 1248-1257
832 (2019).
833 25. S. T. Schafer *et al.*, Pathological priming causes developmental gene network
834 heterochronicity in autistic subject-derived neurons. *Nat Neurosci* **22**, 243-255 (2019).
835 26. F. Birey *et al.*, Assembly of functionally integrated human forebrain spheroids. *Nature* **545**,
836 54-59 (2017).
837 27. S. J. Yoon *et al.*, Reliability of human cortical organoid generation. *Nat Methods* **16**, 75-
838 78 (2019).
839 28. T. A. Khan *et al.*, Neuronal defects in a human cellular model of 22q11.2 deletion
840 syndrome. *Nat Med* **26**, 1888-1898 (2020).
841 29. H. R. Willsey *et al.*, Parallel in vivo analysis of large-effect autism genes implicates cortical
842 neurogenesis and estrogen in risk and resilience. *Neuron* **109**, 1409 (2021).

843 30. B. Gegenhuber, M. V. Wu, R. Bronstein, J. Tollkuhn, Gene regulation by gonadal hormone
844 receptors underlies brain sex differences. *Nature* **606**, 153-159 (2022).
845 31. T. C. Roberts, R. Langer, M. J. A. Wood, Advances in oligonucleotide drug delivery. *Nature*
846 *Reviews Drug Discovery* **19**, 673-694 (2020).
847 32. R. Sebastian *et al.*, Schizophrenia-associated NRXN1 deletions induce developmental-
848 timing- and cell-type-specific vulnerabilities in human brain organoids. *Nature*
849 *Communications* **14**, 3770 (2023).
850 33. L. Zeng *et al.*, Functional impacts of NRXN1 knockdown on neurodevelopment in stem
851 cell models. *PLoS One* **8**, e59685 (2013).
852 34. M. Birtele *et al.*, The autism-associated gene SYNGAP1 regulates human cortical
853 neurogenesis. *bioRxiv*, 2022.2005.2010.491244 (2022).
854 35. J. H. Trotter *et al.*, Astrocytic Neurexin-1 Orchestrates Functional Synapse Assembly.
855 *BioRxiv*, (2020).
856 36. S. Ingusci, G. Verlengia, M. Soukupova, S. Zucchini, M. Simonato, Gene Therapy Tools
857 for Brain Diseases. *Frontiers in pharmacology* **10**, (2019).
858 37. J.-B. Brunet de Courssou, A. Durr, D. Adams, J.-C. Corvol, L.-L. Mariani, Antisense
859 therapies in neurological diseases. *Brain* **145**, 816-831 (2022).
860 38. C. Yilmaz *et al.*, Neurosteroids as regulators of neuroinflammation. *Frontiers in*
861 *Neuroendocrinology* **55**, 100788 (2019).
862 39. E. National Academies of Sciences, Medicine, *Sex Differences in Brain Disorders:*
863 *Emerging Transcriptomic Evidence: Proceedings of a Workshop*. L. Bain, S. M. P. Norris,
864 C. Stroud, Eds., (The National Academies Press, Washington, DC, 2021), pp. 62.
865 40. A. Jack *et al.*, A neurogenetic analysis of female autism. *Brain* **144**, 1911-1926 (2021).
866 41. D. M. Werling, The role of sex-differential biology in risk for autism spectrum disorder. *Biol*
867 *Sex Differ* **7**, 58 (2016).
868 42. E. J. Hoffman *et al.*, Estrogens Suppress a Behavioral Phenotype in Zebrafish Mutants of
869 the Autism Risk Gene, CNTNAP2. *Neuron* **89**, 725-733 (2016).
870 43. M. M. McCarthy, Estradiol and the developing brain. *Physiol Rev* **88**, 91-124 (2008).
871 44. C. S. Woolley, Acute Effects of Estrogen on Neuronal Physiology. *Annual Review of*
872 *Pharmacology and Toxicology* **47**, 657-680 (2007).
873 45. H. C. Lin *et al.*, NGN2 induces diverse neuron types from human pluripotency. *Stem Cell*
874 *Reports* **16**, 2118-2127 (2021).
875 46. F. Zafra, D. Piniella, Proximity labeling methods for proteomic analysis of membrane
876 proteins. *Journal of Proteomics* **264**, 104620 (2022).

877 47. L. Wang *et al.*, Analyses of the autism-associated neuroligin-3 R451C mutation in human
878 neurons reveal a gain-of-function synaptic mechanism. *Molecular psychiatry*, (2022).
879 48. A. Pinggera *et al.*, New gain-of-function mutation shows CACNA1D as recurrently mutated
880 gene in autism spectrum disorders and epilepsy. *Hum Mol Genet* **26**, 2923-2932 (2017).
881 49. M. B. Clark *et al.*, Long-read sequencing reveals the complex splicing profile of the
882 psychiatric risk gene CACNA1C in human brain. *Molecular psychiatry* **25**, 37-47 (2020).
883 50. S. J. Sanders *et al.*, Progress in Understanding and Treating SCN2A-Mediated Disorders.
884 *Trends in neurosciences* **41**, 442-456 (2018).
885 51. S. A. Sloan, J. Andersen, A. M. Pasca, F. Birey, S. P. Pasca, Generation and assembly
886 of human brain region-specific three-dimensional cultures. *Nat Protoc*, (2018).
887 52. A. Nicolas *et al.*, Genome-wide Analyses Identify KIF5A as a Novel ALS Gene. *Neuron*
888 **97**, 1268-1283 e1266 (2018).
889 53. A. Dobin *et al.*, STAR: ultrafast universal RNA-seq aligner. *Bioinformatics* **29**, 15-21
890 (2013).
891 54. Y. Liao, G. K. Smyth, W. Shi, featureCounts: an efficient general purpose program for
892 assigning sequence reads to genomic features. *Bioinformatics* **30**, 923-930 (2014).
893 55. M. D. Robinson, D. J. McCarthy, G. K. Smyth, edgeR: a Bioconductor package for
894 differential expression analysis of digital gene expression data. *Bioinformatics* **26**, 139-
895 140 (2010).
896 56. G. E. Hoffman *et al.*, Transcriptional signatures of schizophrenia in hiPSC-derived NPCs
897 and neurons are concordant with post-mortem adult brains. *Nat Commun* **8**, 2225 (2017).
898 57. A. M. Newman *et al.*, Determining cell type abundance and expression from bulk tissues
899 with digital cytometry. *Nature biotechnology* **37**, 773-782 (2019).
900 58. G. E. Hoffman, E. E. Schadt, variancePartition: interpreting drivers of variation in complex
901 gene expression studies. *BMC bioinformatics* **17**, 483 (2016).
902 59. M. E. Ritchie *et al.*, limma powers differential expression analyses for RNA-sequencing
903 and microarray studies. *Nucleic Acids Res* **43**, e47 (2015).
904 60. N. L. Bray, H. Pimentel, P. Melsted, L. Pachter, Near-optimal probabilistic RNA-seq
905 quantification. *Nature biotechnology* **34**, 525-527 (2016).
906 61. I. De Marinis, P. Lo Surdo, G. Cesareni, L. Perfetto, SIGNORApp: a Cytoscape 3
907 application to access SIGNOR data. *Bioinformatics* **38**, 1764-1766 (2022).
908 62. T. Stuart *et al.*, Comprehensive Integration of Single-Cell Data. *Cell* **177**, 1888-1902 e1821
909 (2019).

910 63. J. Urresti *et al.*, Correction: Cortical organoids model early brain development disrupted
911 by 16p11.2 copy number variants in autism. *Mol Psychiatry* **26**, 7581 (2021).
912 64. X. Yang *et al.*, Identification and validation of genes affecting aortic lesions in mice. *J Clin*
913 *Invest* **120**, 2414-2422 (2010).
914 65. K. Stefan, J. W. Harbour, SparK: A Publication-quality NGS Visualization Tool. *bioRxiv*,
915 845529 (2019).
916

Supplement for *Fernando et al., 2023*

		CONTROL				5'-DEL		3'-DEL		Genotype
										Data Point Color
Reference	Experiment	553-3	2607-4	3182-3	690-2	972-5	973-5	581-5	641-6	Donor Cell Line-Clone
Fig. 1 & Fig. S2	iGLUT/ iGABA generation	✓	✓	✓	✓	✓	✓	✓	✓	
	Immunostaining	✓	✓							
	Case/Control RNASeq	✓	✓			✓	✓	✓	✓	
Fig. 2 & Fig. S3	Case/Control MEA iGLUT	✓	✓			✓	✓	✓	✓	
	Case/Control MEA iGABA	✓	✓	✓	✓	✓	✓	✓	✓	
	Patch-Clamp iGLUT (Excitability)	✓	✓			✓	✓	✓	✓	
	Patch-Clamp iGABA (Excitability)	✓	✓			✓	✓	✓	✓	
Fig. S4	KCC2 MEA (GABAZine)			✓	✓					
Fig. 3	Patch-Clamp iGLUT (Neurotransmitter release)	✓	✓	✓	✓	✓	✓	✓	✓	
Fig. 3	Patch-Clamp iGABA (Neurotransmitter release)	✓	✓			✓	✓	✓	✓	
Fig. S5	TTX Experiments iGLUT	✓	✓			✓	✓	✓	✓	
Fig. S5	TTX Experiments iGABA	✓	✓		✓	✓	✓	✓	✓	
Fig. 4, Fig. S6 & S7	Organoid generation	✓	✓			✓	✓	✓	✓	
	Organoid characterization	✓	✓			✓	✓	✓	✓	
	Organoid rosette imaging	✓	✓			✓	✓	✓	✓	
	Organoid single cell sequencing	✓*	✓			✓	✓	✓	✓	
Fig. 5 & Fig S8.	shRNA testing iGLUT-WT	✓	✓	✓	✓					
	shRNA patch-clamp iGLUT-WT				✓					
	shRNA testing iGABA-WT	✓	✓	✓	✓					
	shRNA patch-clamp iGABA-WT		✓	✓	✓					
	shRNA testing iGLUT-MT							✓	✓	
	shRNA patch-clamp iGLUT-MT							✓		
	shRNA testing iGABA-MT							✓	✓	
	shRNA patch-clamp iGABA-MT							✓		
Fig. 5	Beta-Estradiol					✓	✓			
Fig. 5	Anti-sense Oligos							✓	✓	

Extended Data Figure 1: *Specific cell lines used in each experiment throughout this study.* Reference table of all cell lines-clones used per experiment with corresponding data point colors. Check marks indicate inclusion for experiments, *represents dropped donor due to failed QC.

a

	iGLUT 5'-Del		iGLUT 3'-Del		iGABA 5'-Del		iGABA 3'-Del	
	Overlapped DEGs with risk genes	Overlapped DEGs with risk genes & in SIGNOR database	Overlapped DEGs with risk genes	Overlapped DEGs with risk genes & in SIGNOR database	Overlapped DEGs with risk genes	Overlapped DEGs with risk genes & in SIGNOR database	Overlapped DEGs with risk genes	Overlapped DEGs with risk genes & in SIGNOR database
ASD	11	**7**	4	**0**	3	**1**	6	**2**
BP	16	**9**	3	**1**	2	**1**	5	**1**
SCZ	26	**14**	10	**1**	9	**3**	14	**3**
Total	37	**22**	12	**2**	9	**3**	18	**4**

b

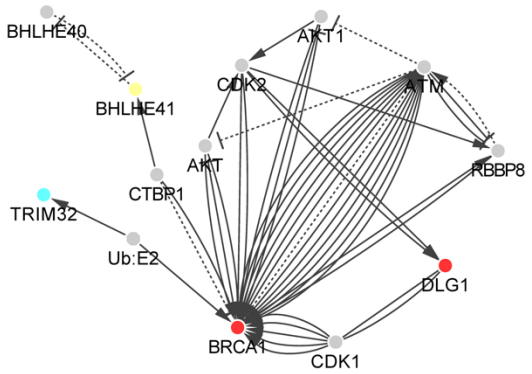

c

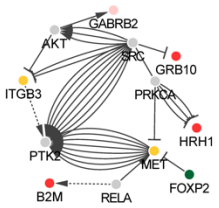

d

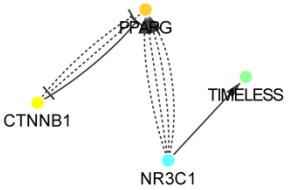

e

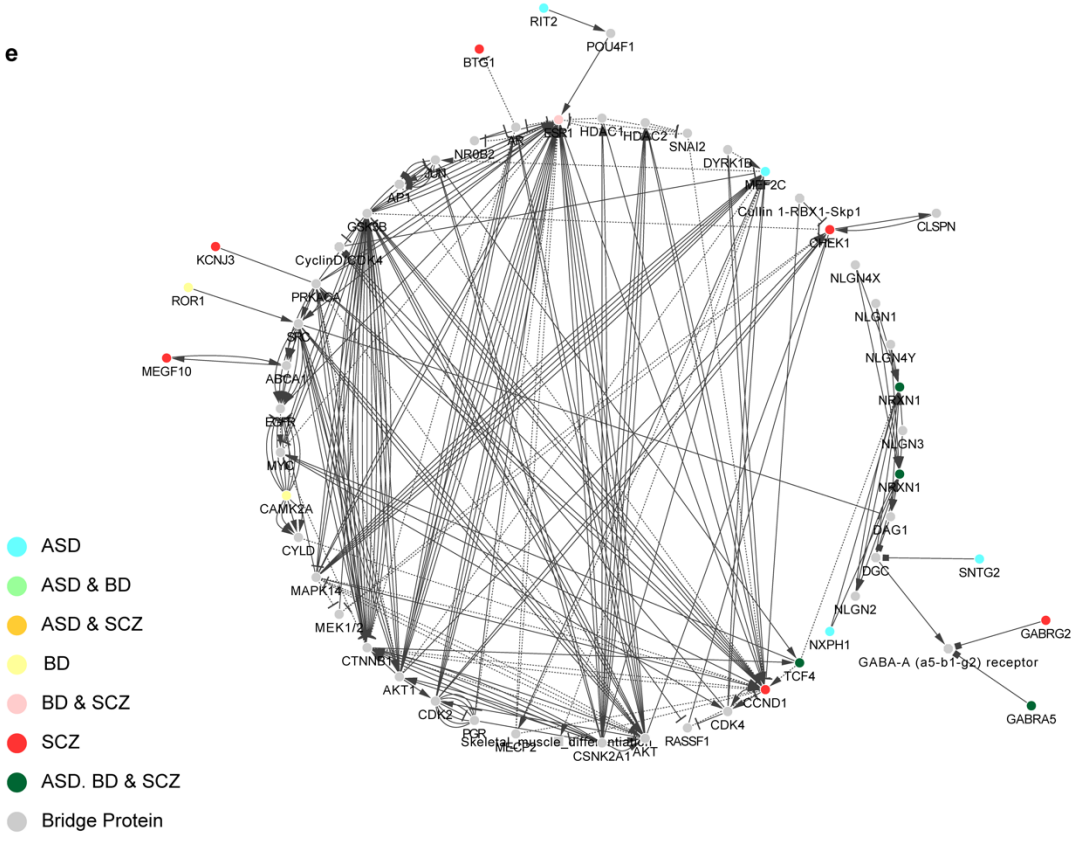

Extended Data Figure 2: *Extended transcriptomics analysis on disease risk associated genes.* (a) Summary table of overlapping DEGs with risk enrichments across publicly curated datasets for autism (ASD), bipolar disorder (BD) and schizophrenia. Interaction maps of risk genes for (b) 3'-Del iGLUT, (c) 3'-Del iGABA, (d) 5'-Del iGABA and (e) 5'-iGLUT. Sample information correspond to Fig. 1

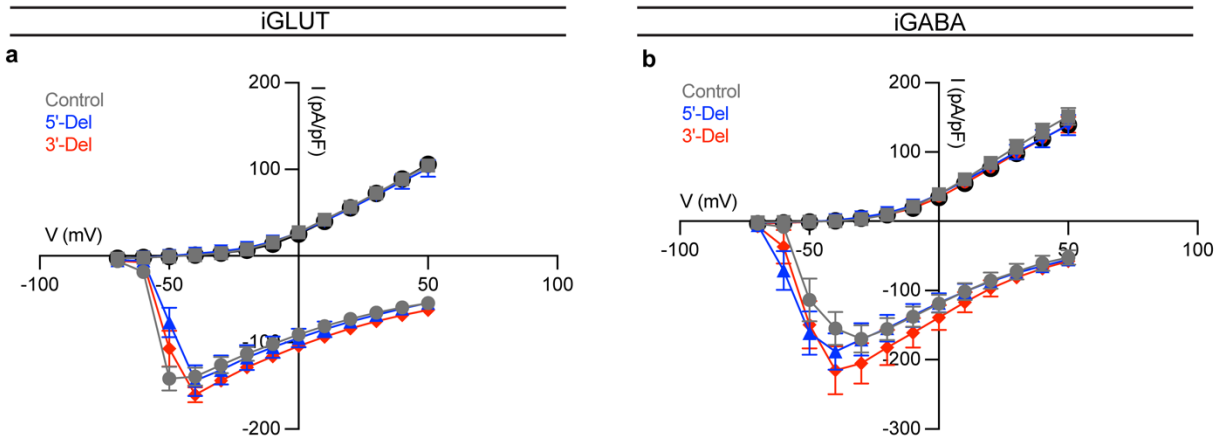

Extended Data Figure 3: *Extended data excitable properties of 5'-Del and 3'-Del neurons.* Voltage-gated potassium and channel kinetics across genotypes for (a) iGLUT (n = 6 donors | 2 inductions | 45 neurons) and (b) iGABA neurons (n = 6 donors | 2 inductions | 34 neurons).

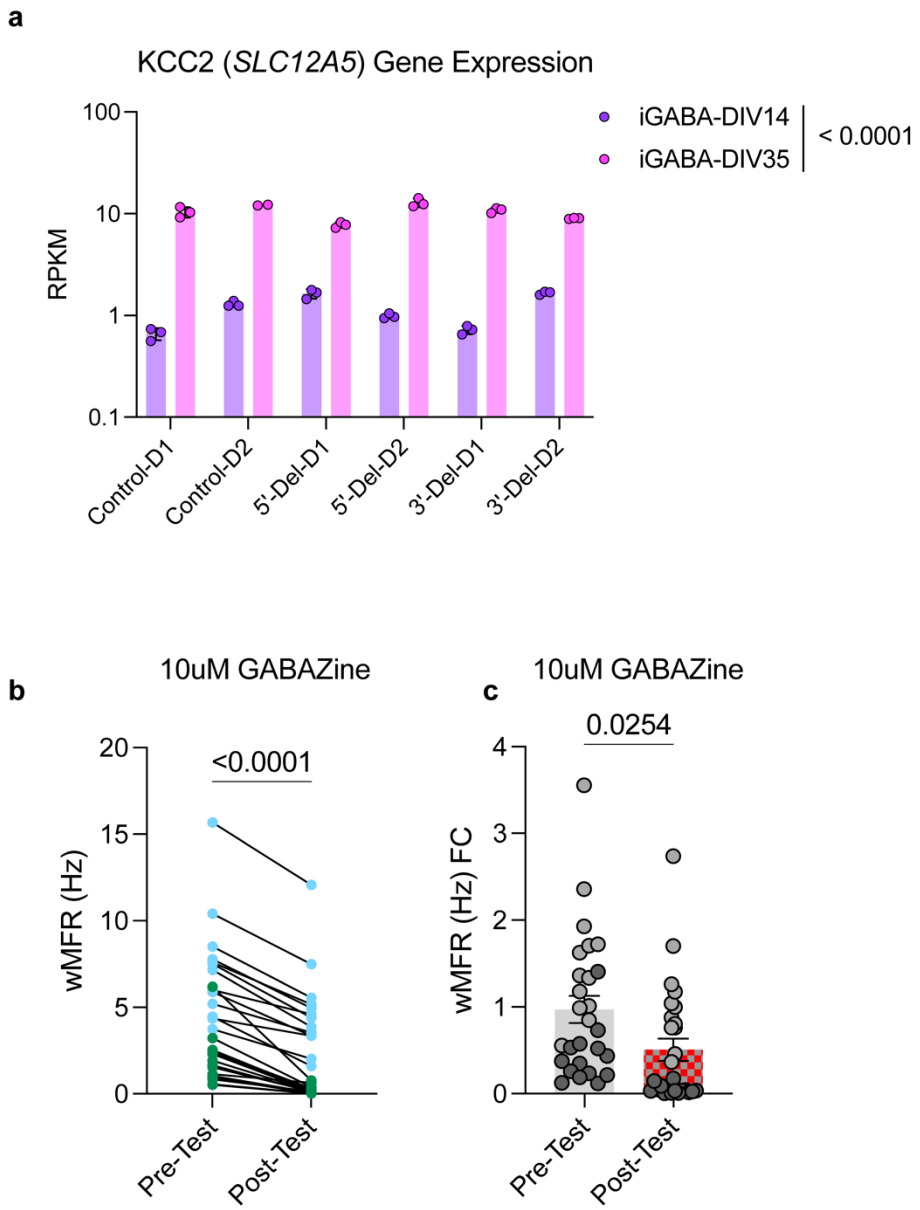

Extended Data Figure 4: *Extended KCC2 related data from immature GABA neurons.* (a) Transcriptomic comparison of *SLC12A5* expression across DIV14 and DIV35 RNASeq timepoints. (b,c) MEA tests from pre- and post- treatment of 10uM GABAzine. (n = 2 donors | 1 representative induction | 28 MEA wells) Statistical tests are paired student's t-test for time-linked comparison and unpaired student's t-test for pre/post activity foldchange.

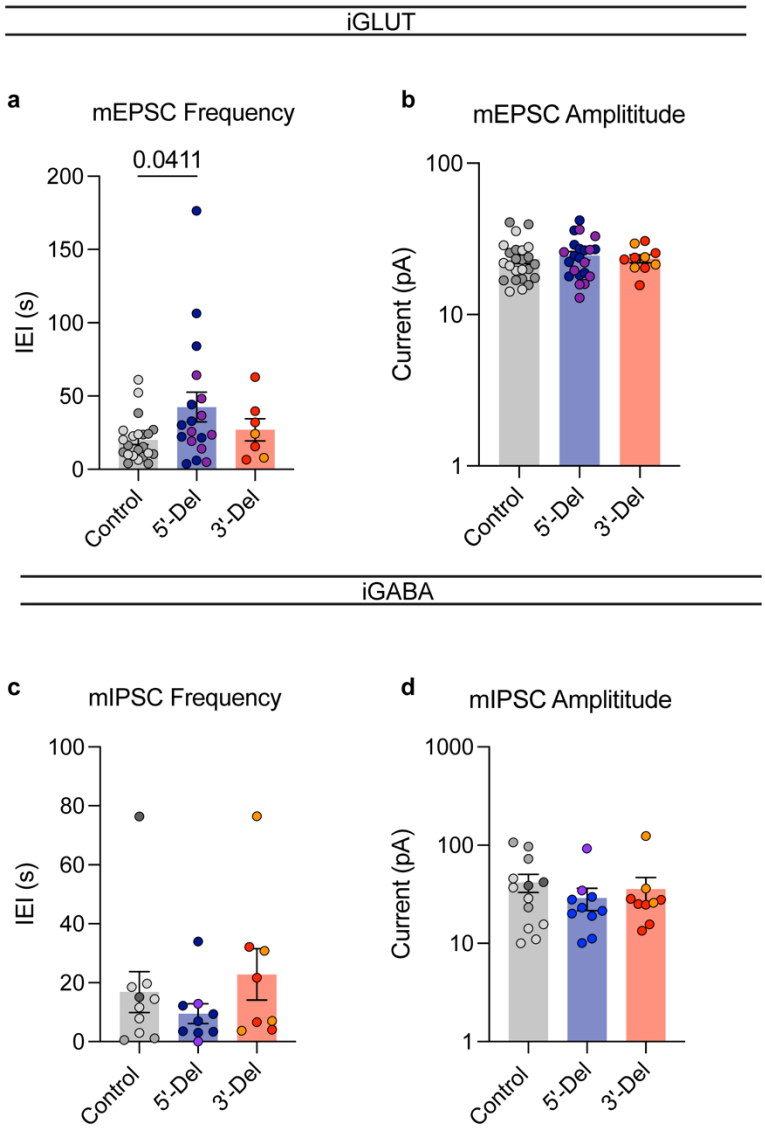

Extended Data Figure 5: *Miniature neurotransmitter release data (+TTX) from iGLUT and iGABA neurons.* Comparative mEPSC kinetics of (a) IEI and (b) amplitude size from iGLUT neurons (n= 6 donors | 4 inductions | 47 neurons). Statistical test used was a 1-way ANOVA with Dunnett's test. Comparative mIPSC kinetics of (a) IEI and (b) amplitude size from iGABA neurons (n= 6 donors | 3 inductions | 27 neurons). Statistical test used was a 1-way ANOVA with Dunnett's test.

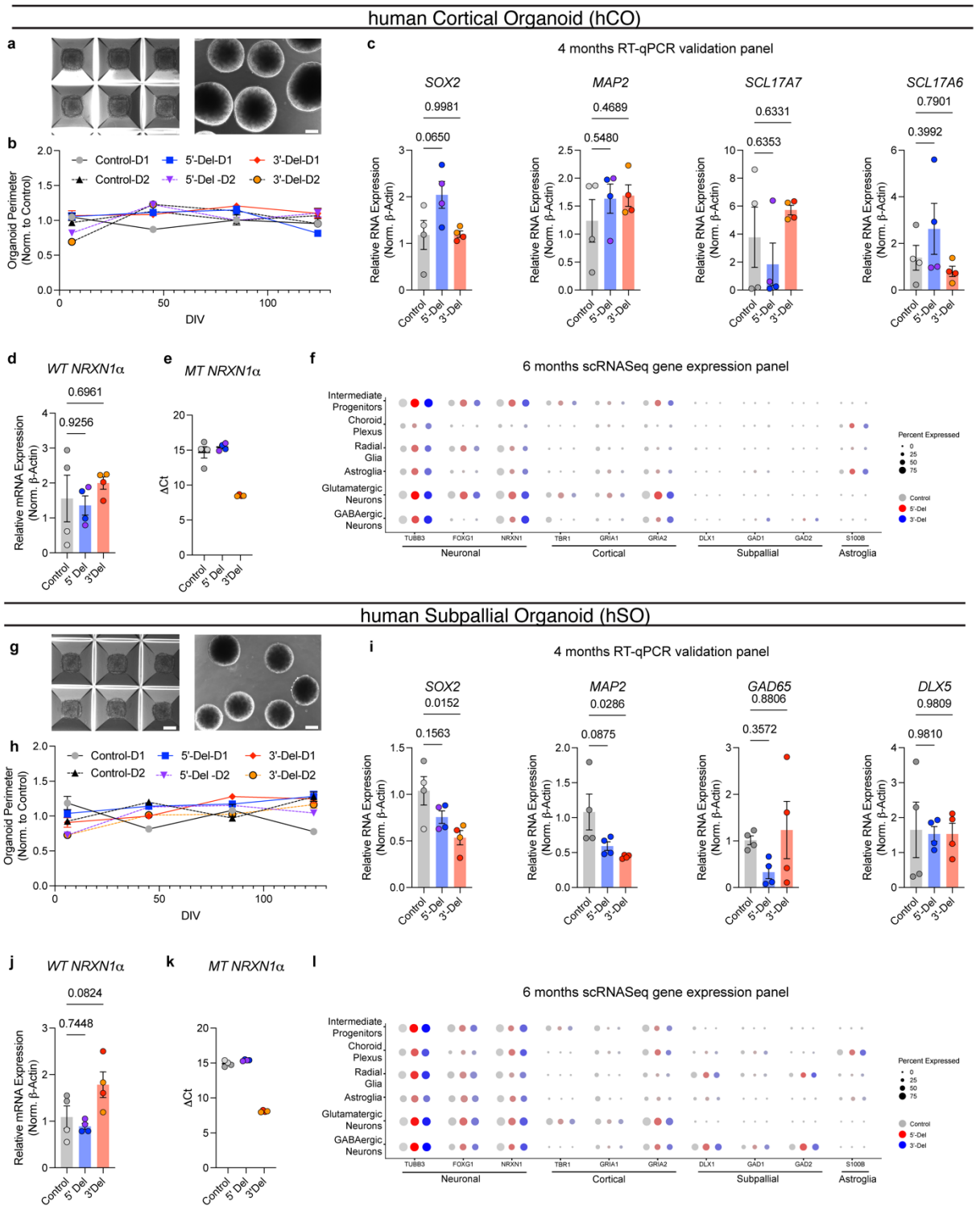
human Cortical Organoid (hCO)
a
b
Control-D1
5'-Del-D1
3'-Del-D1
Control-D2
5'-Del -D2
3'-Del-D2
Organoid Perimeter (Norm. to Control)
DIV
c
4 months RT-qPCR validation panel
SOX2
0.9981
0.0650
MAP2
0.4689
0.5480
SCL17A7
0.6331
0.6353
SCL17A6
0.7901
0.3992
Relative RNA Expression (Norm. β-Actin)
Control
5'-Del
3'-Del
d
WT NRXN1α
0.6961
0.9256
Relative mRNA Expression (Norm. β-Actin)
e
MT NRXN1α
ΔCt
f
6 months scRNASeq gene expression panel
Intermediate Progenitors
Choroid Plexus
Radial Glia
Astroglia
Glutamatergic Neurons
GABAergic Neurons
TUBB3
FOXG1
NRXN1
TBR1
GRIA1
GRIA2
DLX1
GAD1
GAD2
S100B
Neuronal
Cortical
Subpallial
Astroglia
Percent Expressed
human Subpallial Organoid (hSO)
g
h
i
4 months RT-qPCR validation panel
SOX2
0.0152
0.1563
MAP2
0.0286
0.0875
GAD65
0.8806
0.3572
DLX5
0.9809
0.9810
j
WT NRXN1α
0.0824
0.7448
k
MT NRXN1α
l
6 months scRNASeq gene expression panel

Extended Data Figure 6: *Extended data on human organoid generation and characterization.* (a,g) Representative images of hiPSC aggregation and immature spheroids post dislodging. (b,h) Normalized organoid perimeters over time (compared to averaged control), hCO (n = 6 donors | 2 batches | 72-161 organoids) and hSO (n = 6 donors | 2 batches | 46-134 organoids). (c, i) RT-qPCR results from 4-month organoids of genes for pluripotency, neuronal, and cell-type specific markers. (d-e, j-k) RT-qPCR results of *NRXN1* WT and MT expression hCO (n = 6 donors | 1 representative batch | 12 samples) and hSO (n = 6 donors | 1 representative batch | 12 samples). Statistical tests used were 1-way ANOVAs with Dunnett's test. (f, l) Comprehensive gene expression panel across sub-clusters of hCO and hSO samples across neuronal, cortical, subpallial and astroglia markers. Data corresponds to Fig 4.

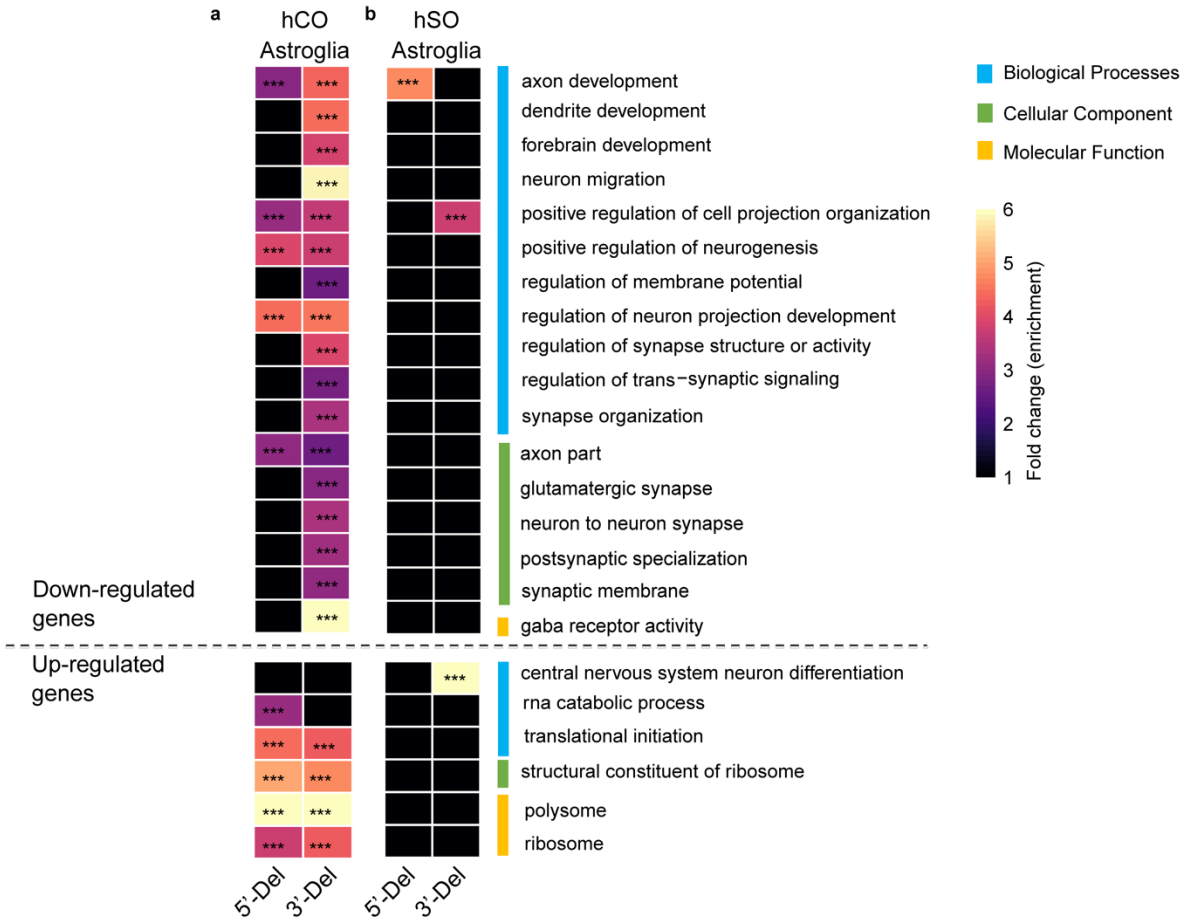

Extended Data Figure 7: *Extended analysis on astroglia subclusters from hCO and hSOs.* (a) hCO subcluster and (b) hCO subcluster GO analysis of overlapped terms with hCO-glutamatergic and hSO-GABAergic enrichments. *P < 0.05, **P < 0.01, ***P <0.001, Wilcoxon's rank sum test, FDR = 0.05.

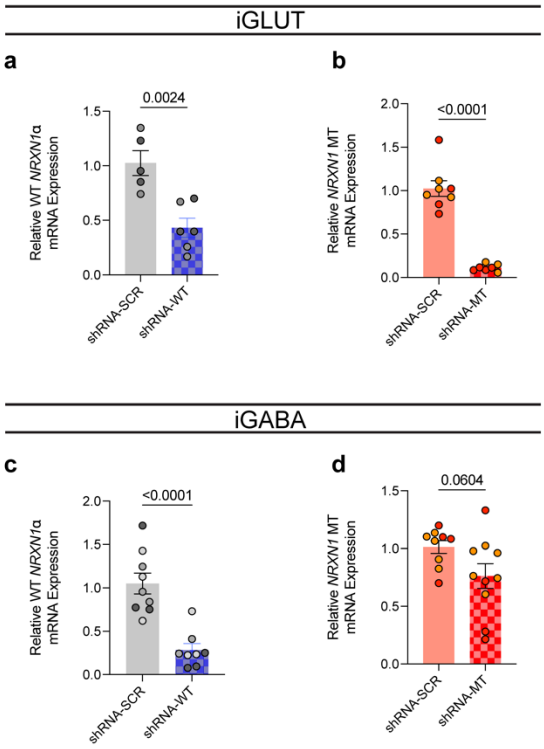

Extended Data Figure 8: *shRNA knockdown validation.* (a) Extent of shRNA knockdown on WT and (b) MT *NRXN1* expression in iGLUT neurons (n = 2 donors | 1-3 inductions). (c) Extent of shRNA knockdown on WT and (d) MT *NRXN1* expression in iGABA neurons, (n = 2-3 donors | 1-3 inductions) Statistical tests used were Student's t-test.

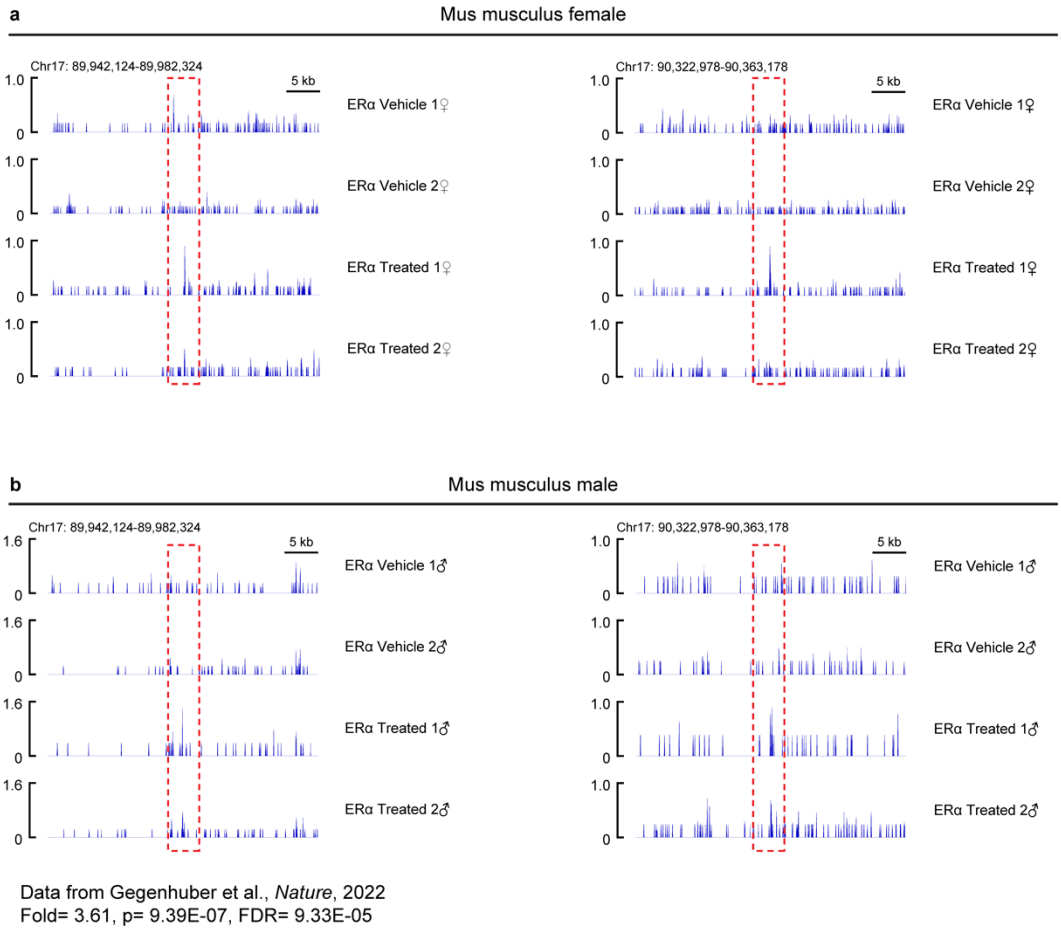

Extended Data Figure 9: *ChIP-seq enrichment of ER1 binding at NRXN1 loci in rodent brain.* (a) Female and (b) male mus musculus ChIP tracts of *NRXN1* locus, with red dashed areas highlighting binding enrichment across vehicle and estradiol treated mice.